Evaluation of Gremlin-1 as a therapeutic target in metabolic dysfunction-associated steatohepatitis

Paul Horn[1,2,3,4], Jenny Norlin[6], Kasper Almholt[6], Birgitte M. Viuff[6], Elisabeth D. Galsgaard[7], Andreas Hald[8], Franziska Zosel[8], Helle Demuth[8], Svend Poulsen[8], Peder L. Norby[8], Morten G. Rasch[8], Mogens Vyberg [9], Marco R. Rink[2], Emma Shepherd[2], Ellie Northall[2], Patricia F. Lalor[2], Chris J. Weston[1,2*], Morten Fog-Tonnesen[6*] and Philip N. Newsome[1,2,5*]

Affiliations:

[1] National Institute for Health Research, Biomedical Research Centre at University Hospitals Birmingham NHS Foundation Trust and the University of Birmingham
[2] Centre for Liver & Gastrointestinal Research, Institute of Immunology and Immunotherapy, University of Birmingham
[3] Department of Hepatology & Gastroenterology, Charité - Universitätsmedizin Berlin, Campus Virchow-Klinikum and Campus Charité Mitte, Berlin, Germany
[4] Berlin Institute of Health at Charité – Universitätsmedizin Berlin, BIH Biomedical Innovation Academy, BIH Charité Digital Clinician Scientist Program, Berlin, Germany
[5] Liver Unit, University Hospitals Birmingham NHS Foundation Trust, Birmingham
[6] Global Drug Discovery, Novo Nordisk A/S, Maaloev, Denmark
[7] Global Translation, Novo Nordisk A/S, Maaloev, Denmark
[8] Global Research Technologies, Novo Nordisk A/S, Maaloev, Denmark
[9] Department of Pathology, Copenhagen University Hospital Hvidovre, and Centre for RNA medicine, Aalborg University Copenhagen, Denmark
* These authors contributed equally

Correspondence:

Prof. Philip N. Newsome, PhD, FRCP
Centre for Liver and Gastrointestinal Research, 5th Floor Institute of Biomedical Research, Wolfson Drive, University of Birmingham, UK, B15 2TT
p.n.newsome@bham.ac.uk

Abstract

Gremlin-1 has been implicated in liver fibrosis in metabolic dysfunction-associated steatohepatitis (MASH) via inhibition of bone-morphogenetic protein (BMP) signalling and has thereby been identified as a potential therapeutic target. Using rat *in vivo* and human *in vitro* and *ex vivo* model systems of MASH fibrosis, we show that neutralisation of Gremlin-1 activity with monoclonal therapeutic antibodies does not reduce liver inflammation or liver fibrosis. Still, Gremlin-1 was upregulated in human and rat MASH fibrosis, but expression was restricted to a small subpopulation of COL3A1/THY1^{+} myofibroblasts. Lentiviral overexpression of Gremlin-1 in LX-2 cells and primary hepatic stellate cells led to changes in BMP-related gene expression, which did not translate to increased fibrogenesis. Furthermore, we show that Gremlin-1 binds to heparin with high affinity, which prevents Gremlin-1 from entering systemic circulation, prohibiting Gremlin-1-mediated organ crosstalk. Overall, our findings suggest a redundant role for Gremlin-1 in the pathogenesis of liver fibrosis, which is unamenable to therapeutic targeting.

Key words: bone-morphogenetic proteins / gremlin-1 / liver fibrosis / metabolic dysfunction-associated steatotic liver disease / metabolic dysfunction-associated steatohepatitis

Introduction

Metabolic dysfunction-associated steatotic liver disease (MASLD) is aetiologically closely linked to insulin resistance and the metabolic syndrome, and in parallel with the rise in obesity is becoming the most common chronic liver disease worldwide, affecting about twenty to thirty percent of the population in western countries (1,2). It is characterised by hepatocellular lipid accumulation and, through multiple mechanisms, can progress to inflammation of the liver (metabolic dysfunction-associated steatohepatitis, MASH) and subsequent fibrosis (3). Liver fibrosis has been identified as the predominant factor determining patient prognosis, and higher stages are associated with liver-related events such as liver failure or the development of hepatocellular carcinoma, as well as extrahepatic events such as cardiovascular disease, extrahepatic cancer or endocrinological complications (4).

Gremlin-1 is a protein that is mainly expressed in fibroblasts and stem cells, and has been linked to fibrosis in a number of organs, including the kidney, lung, pancreas and skin (5–8). It acts mainly via inhibition of bone morphogenetic protein (BMP) signalling by direct binding and inactivation of BMPs 2, 4, and 7 (9), whilst some reported actions on vascular endothelial growth factor receptor 2 (VEGFR2) and monocyte migration inhibitory factor (MIF) (10,11). Gremlin-1 forms dimers and avidly binds to glycosaminoglycans such as heparin and heparan sulphate, although the latter is not necessary for its interaction with BMPs (12–15). In the liver, expression generally is low (16) and restricted to activated hepatic stellate cells, which are the main fibrogenic cell population in the liver along with fibroblasts (17,18). Hepatic Gremlin-1 has been linked to hepatocellular insulin resistance (19) and recent literature described a role in driving hepatocellular senescence, which in turn is linked to hepatic fibrogenesis and carcinogenesis (20). Previous evidence suggests that Gremlin-1 plays an active role in liver fibrosis by inhibiting the anti-fibrotic action of

78 BMPs 4 and 7 on activated hepatic stellate cells (21,22). Systemic siRNA-mediated
79 knockdown of Gremlin-1 downregulated hepatic TGFβ signalling and reduced fibrosis
80 in a rat CCl_4 model of liver fibrosis (22). Furthermore, adipose tissue dysfunction and
81 inflammation are both important factors in the pathogenesis of MASLD and MASH
82 fibrosis (23), and Gremlin-1 has been described to drive adipogenesis and adipocyte
83 dysfunction in hypertrophic adipose tissue (24).

84 However, to date the effects of therapeutic inhibition of Gremlin-1 in human liver
85 fibrosis, and MASH in particular, have not been studied. In this study, we aimed to
86 further characterize the expression of Gremlin-1 in human and rodent MASH and
87 evaluate the therapeutic efficacy of an anti-Gremlin-1-directed antibody treatment in
88 rodent and human *in vivo* and *ex vivo* models of MASH fibrosis.

Results

Hepatic gremlin-1 is increased in human and rat MASH liver, localised to portal myofibroblasts

We wanted to determine Gremlin-1 expression in MASH and establish which, if any, cell types in the liver expressed Gremlin-1. Gremlin-1 was undetectable in healthy human liver by RNAscope *in situ* hybridization (ISH) but staining increased in fibrotic NMSH liver, localising to fibrotic septa (Figure 1A and B). Therefore, we hypothesized that Gremlin-1 is involved in hepatic fibrogenesis and that its expression might correlate with advancing stages of fibrosis in MASH. By RTqPCR of human explant livers of different aetiologies (all fibrosis stage F4), we found 4.8 to 9.8-fold increased GREM1 mRNA expression in MASH, ALD, PBC and PSC liver tissues when compared to donor livers (n=13-15 each, Figure 1C). Notably though, when analyzing publicly available bulk RNA sequencing from a total of 352 patients with MASLD (n=58 E-MTAB-9815, n=78 GSE130970, n=216 GSE135251), capturing the whole spectrum of MASLD and MASH, we found no correlation of GREM1 expression with the histological stage of fibrosis (Supplemental Figure 1).

GREM1 mRNA positive cells also stained positive for THY1 and COL3A1 in RNAscope ISH (Figure 1D), indicating that myofibroblasts in the fibrotic area were the major cell type expressing Gremlin-1 in human MASH. This was corroborated by findings from RTqPCR on cultured hepatic cells where GREM1 mRNA expression was highest in primary human hepatic stellate cells and myofibroblasts as compared to absent or low expression in biliary epithelial and sinusoidal endothelial cells (Figure 1E). However, only a small proportion of THY1/COL3A1^{+} cells expressed GREM1, with expression being highly variable across and within each specimen. In agreement, integrated analyses of two publicly available single-cell RNA sequencing

data sets overall showed very low expression levels of Gremlin-1 across cell types (Supplemental Figure 2A-C), but slightly higher expression in THY1 and COL3A1-expressing myofibroblast populations and smooth muscle cells (Supplemental Figure 2D-F).

In order to find a suitable animal model for studying therapeutic effects of neutralizing Gremlin-1, we sought to establish whether rodent MASH models adequately reflect the changes in hepatic GREM1 expression we observed in human MASH. We found no evidence of consistent Grem1 expression in healthy and fibrotic mouse liver tissues (not shown). However, Grem1 ISH staining was consistently increased in livers of rats fed a choline-deficient, L-amino acid defined high-fat diet (CDAA-HFD) for twelve weeks. Like our observations in human MASH liver tissue, Grem1 expression in rat livers mainly localised to periportal fibrotic areas (Figure 1F).

Gremlin-1 is undetectable in the circulation, due to avid glycosaminoglycan binding

Increased circulating Gremlin-1 protein has been described in patients with type 2 diabetes and in MASH and has been linked to higher MASH disease severity (19). Therefore, we wanted to verify these findings and investigate whether circulating Gremlin-1 protein also correlates with the stage of fibrosis. We developed a luminescent oxygen channelling immunoassay (LOCI, alphaLISA) using different combinations of in-house generated human recombinant anti-Gremlin-1 antibodies. These assays were highly sensitive, with a lower limit of quantification of 0.1 ng/mL, and highly specific as suggested by the absence of any signal. However, despite high sensitivity, we were unable to detect circulating Gremlin-1 in plasma or serum in a cohort of healthy subjects and MASLD patients with different stages of fibrosis

(Figure 2A and B, clinical characteristics see Table 1). Using size exclusion chromatography, we observed that dimeric Gremlin-1 forms dimers and trimers in complex with heparin under cell- and matrix-free conditions (Figure 2C), suggesting that Gremlin-1 might be retained on cell surfaces and extracellular matrix and thus not enter the systemic circulation. Furthermore, the binding affinity of Gremlin-1 to heparin was in the low nanomolar range (Figure 3E), suggesting a strong localization towards extracellular matrix proteoglycans.

Development and characterisation of a neutralising anti-Gremlin-1 directed antibody

Given the potential role of Gremlin-1 in hepatic fibrogenesis in MASH, we developed therapeutic anti-Gremlin-1 antibodies and aimed to test whether neutralization of Gremlin-1 interfered with fibrosis in models of MASH. Generated antibodies were highly effective in blocking recombinant human Gremlin-1 from binding BMP4 in a Gremlin/BMP4 inhibition ELISA (Figure 3A, IC50 = 2.7-3.1x10^{-9}M) as well as in a BRE-Luc RGA BMP reporter assay (Figure 3B, EC50 = 1.27-1.36x10^{-8}M) with IC50/EC50 values being the lowest possible that can be reached given the amount of Gremlin-1 used in the assays. Treatment of LX-2 cells with BMP4 also increased SMAD1 phosphorylation, which was prevented by the addition of Gremlin-1 (Figure 3C), and anti-Gremlin-1 antibodies, but not isotype control, effectively restored SMAD1 phosphorylation in a dose-dependent manner (Figure 3C, K_D = 2.04-2.96x10^{-9} M). Antibodies differed in their binding stoichiometries; the 0032:ND/0568:ND antibody formed complexes with Gremlin-1 dimers in a 2:2 ratio, whilst the 0030:HD compound bound Gremlin-1 predominantly in a 1:1 ratio (Figure 3D).

Antibodies had different effects with regards to heparin binding, indicated by suffixes HD for heparin-displacing and ND for non-displacing antibodies. Using a fluorescence polarization assay we found that Gremlin-1 bound to heparin with high affinity (Figure 3E, K_D [Grem1 alone] = 13 nM), confirming our chromatography findings. Whilst the 0032:ND compound did not affect heparin binding of Gremlin-1, the 0030:HD heparin-displacing antibody reduced the affinity by a factor of ten (K_D [0032:ND- Gremlin-1] = 18 nM *vs* K_D [0030:HD- Gremlin-1] = 99 nM, respectively, Figure 3E). In line with these results, Atto-532-conjugated Gremlin-1 bound to the cell surface of LX-2 cells which was prevented by the heparin-displacing 0030:HD but not the 0032:ND or isotype control antibody (Figure 3F). Size-exclusion chromatography on mixtures of Gremlin-1, heparin and anti-Gremlin-1 antibodies revealed that the 0030:HD antibody forms 1:1 complexes with free Gremlin-1 not involving heparin, while the 0032:ND antibody captures heparin-bound Gremlin-1, leading to the formation of higher-order complexes that were insoluble and precipitated (Supplemental Figure 3).

Overexpression but not antibody blockade of Gremlin-1 modified the expression profile of human hepatic fibrogenic cells

Having characterised effective neutralising antibodies against Gremlin-1, we evaluated whether anti-Gremlin-1 treatment reduced the fibrogenic activation of hepatic stellate cells. For this purpose we used the heparin-displacing 0030:HD antibody. However, anti-Gremlin-1 blockade did not change the expression of COL1A1, ACTA2 or TIMP1 either without or with TGFβ1 treatment, when compared to isotype control in primary human hepatic stellate cells (HHSC) or myofibroblasts ($p > 0.05$, Figure 4A and B, respectively). To test whether Gremlin-1 had any impact

on hepatic stellate cell biology, we overexpressed GREM1 on LX-2 cells and HHSC using a second-generation lentiviral vector. Overexpression increased the expression of GREM1 by a factor of 177 after sorting for GFP in LX-2 ($p < 0.001$, Supplemental Figure 4) and by a factor of 6.3 in unsorted HHSC ($p = 0.0204$, Supplemental Figure 4). To assess the effects of overexpression on fibrogenic gene expression, we treated lentivirally transduced cells with TGFβ1 or PBS as vehicle control and performed qPCR for fibrogenic and BMP-signalling-related targets. Overexpression did not significantly affect the expression of COL1A1, ACTA2 or TIMP1 in either LX-2 or primary HHSC (all $p > 0.05$, Figure 4C and D). However, in LX-2 cells, GREM1 overexpression significantly increased the expression LOX in vehicle control treated cells only ($p = 0.020$, Figure 4D), while CCL2 and LOXL1 expression were unaffected ($p = 0.11$ and $p = 0.15$, respectively). Moreover, GREM1 overexpression affected gene expression of several BMP-related signalling targets; BMP4, SMAD6 and SMAD7 expression were reduced in vehicle-treated cells only ($p = 0.016$, $p = 0.013$ and $p = 0.032$, respectively, Figure 4E). Additionally, GREM1 overexpression resulted in a significant downregulation of INHBB expression irrespective of TGFβ1 co-treatment ($p = 2.4 \times 10^{-5}$) and upregulation of BMP7 and SMAD1 ($p = 0.008$ and $p = 0.007$, respectively, Figure 4E).

Lack of therapeutic efficacy in a rat model of MASH fibrosis

To investigate whether therapeutic targeting of hepatic Gremlin-1 could reduce fibrosis in rodent MASH, we used a choline-deficient, L-amino acid defined high fat 1% cholesterol diet (CDAA-HFD) rat model of MASH, in which we had observed increased Gremlin-1 expression. Eight to ten-week-old male Sprague Dawley rats were fed a CDAA-HFD for a total of 12 weeks. In the last six weeks of feeding, rats

were treated with weekly subcutaneous injections of “murinised” monoclonal anti-Gremlin-1 non-heparin-displacing (0361:ND) or heparin-displacing antibody (2021:HD) at different concentrations (Figure 5A). Isotype matched mouse IgG1 antibody served as a control treatment. As expected, CDAA-HFD led to a reduction in body weight and induced a MASH phenotype, as evidenced by increased plasma levels of alanine- and aspartate aminotransferase (ALT and AST, respectively), increased liver weight, steatosis, picrosirius red (PSR) positive fibrosis area and $CD45^+$ immune cell infiltrates (Figure 5B-H).

To test for target engagement of therapeutic antibodies, we took blood at different timepoints of treatment and measured circulating Gremlin-1 concentrations. We did not find any Gremlin-1 protein in rats treated with isotype controls or non-heparin-displacing antibodies, but Gremlin-1 concentration increased with heparin-displacing antibody treatment (Supplemental Figure 5), suggesting that Gremlin-1 was removed from extracellular matrix and entered circulation. However, treatment with either the heparin-displacing or non-displacing antibody did not change MASH phenotype, as measured by serum ALT or AST, liver weight, steatosis, PSR positive area or $CD45^+$ cell infiltrate (all $p > 0.05$, Figure 5C-H). We observed a similar pattern for additional immunohistochemistry read-outs COL1A1, αSMA, CD68, and CD11b (Supplemental Figure 6), and qPCR results for Grem1, Col1a1, Col3a1, Timp1, Tgfb1 and Tnf (Supplemental Figure 7). Quantification results for all antibody concentrations can be found in the Supplementary Materials (Suppl. Table 1 and 2).

Exposure of human cirrhotic precision-cut liver slices to anti-Gremlin-1 antibodies had no impact on the fibrotic response

To test whether anti-Gremlin-1 was effective in a human model system of MASH fibrosis, we treated human PCLS prepared from cirrhotic livers with the human heparin-displacing antibody 0030:HD (Figure 6A). Albumin concentrations and AST activity in supernatants were similar between treatment groups, indicating no toxicity of any of the compounds ($p = 0.358$ and $p = 0.112$, respectively, Supplemental Figure 8). Treatment with TGFβ1 increased the expression of COL1A1, ACTA2 and TIMP1 ($p = 0.033$, $p = 0.095$ and $p = 0.047$, respectively, Figure 6B), while ALK5 inhibition significantly decreased their expression ($p = 9.9x10^{-4}$, $p = 0.040$ and $p = 0.003$, respectively, Figure 6B). The anti-Gremlin-1 antibody did not reduce fibrotic marker expression when compared to the isotype control antibody ($p > 0.283$ in all comparisons, Figure 6B). Concordant with gene expression data, we also saw no changes in soluble Pro-collagen 1A1 levels in PCLS supernatant upon treatment with the anti-Gremlin-1 antibody (Figure 6C). Like for the target engagement studies in the rat CDAA-HFD model, we measured Gremlin-1 protein in PCLS supernatants but were unable to pick up any signal (Supplemental Figure 9A). However, using confocal microscopy on PCLS stained with AF488-conjugated non-heparin displacing antibody, we observed binding of the therapeutic antibody but not the isotype control to scar tissue in PCLS, suggesting adequate tissue penetration (Supplemental Figure 9B). To check whether anti-Gremlin-1 treatment affected other pathways, we performed 3'-mRNA sequencing on antibody-treated PCLS, but differential gene expression analysis did not show any considerable gene expression changes in response to anti-Gremlin-1 treatment (Figure 6D and E).

Discussion

In recent years, Gremlin-1 has been recognised as a potential therapeutic target in treating patients with MASH, and MASH fibrosis in particular. Baboota *et al* recently suggested that anti-Gremlin-1 based therapies may be able to halt or even reverse MASH progression through inhibition of hepatocellular senescence (20). In the present study, we aimed to develop and evaluate anti-Gremlin-1 neutralising antibodies as therapeutic assets for the treatment of MASH fibrosis.

Gremlin-1 is mainly expressed in adipose tissue, the intestine and the kidneys, while hepatic expression is considered low in healthy human (16) and rodent tissue (17). In healthy mouse liver, Gremlin-1 expression was undetectable, but others have previously found increased mRNA expression in murine fibrotic liver in $Mdr2^{-/-}$ mice fed a cholate-containing diet (17) and porcine serum-induced murine liver fibrosis (21). Similarly, in patients with type 2 diabetes and MASH, Hedjazifar *et al* have found increased Gremlin-1 expression and a positive correlation with liver steatosis, inflammation, ballooning and the stage of fibrosis (19). Our findings of increased RNAscope ISH signal in human and rat MASH fibrosis largely corroborate existing evidence, although our secondary analyses from existing bulk RNA-sequencing datasets conflicted in that regard. Furthermore, our RNAscope studies on human livers highlight the heterogeneity of Gremlin-1 expression across and within individual livers, resulting in a high risk of sampling bias. Not least, we showed increased hepatic Gremlin-1 expression across different aetiologies of end-stage chronic liver disease, pointing towards a role not specific to metabolic liver disease.

The exact cellular localisation of hepatic Gremlin-1 is under continuous investigation. Using RNAscope in-situ hybridization, we found that Gremlin-1 mRNA localised to COL3A1/$THY1^{+}$ myofibroblasts. Some authors previously found increased Gremlin-1

expression in human HSC-derived myofibroblasts when compared to quiescent and early activated HSC (17,18). However, following studies found evidence that Gremlin-1 expression is most abundant in portal fibroblasts when compared to hepatic stellate cells in murine bile duct ligation and CCl_4 models of fibrosis (25), suggesting that portal fibroblast-derived myofibroblasts, rather than HSC-derived myofibroblasts, are the predominant Gremlin-1-expressing cells of the liver. Still, as mentioned above, hepatic Gremlin-1 expression seems to be very low, evidenced by available liver scRNA-seq data (26,27). In our integrated analysis of both data sets, Gremlin-1 was barely detectable but showed considerable expression in smooth muscle cell subsets and myofibroblasts expressing COL3A1 and THY1. All taken together, our data confirmed a subset of myofibroblasts as the predominant hepatic cell population expressing Gremlin-1.

We found increased levels of Gremlin-1 expression in MASH fibrosis and localisation of Gremlin-1 to periportal hepatic fibroblasts. However, we did not find any therapeutic effect of antibody-mediated neutralisation of Gremlin-1, neither in a rat CDAA-HFD *in vivo* model nor in human *ex vivo* or *in vitro* culture models of MASH fibrosis. We extensively tested and characterised our therapeutic antibodies and were able to show high-affinity binding to Gremlin-1 and inhibition of its functional activity on BMP4. Furthermore, treating rats with the heparin-displacing anti-Gremlin-1 antibody *in vivo* led to a significant increase in circulating Gremlin-1 protein, evidencing reliable target engagement. However, the small subset of COL3A1+/THY1+ periportal fibroblasts unlikely represents the major fibrogenic cell subset in MASH. While periportal myofibroblasts play an important role in biliary fibrosis (28), in most chronic liver diseases such as MASH and alcohol-related liver disease, hepatic stellate cell (HSC)-derived myofibroblasts represent the predominant fibrogenic cell population (29). Moreover, hepatic Gremlin-1 expression

is quite low when compared to organs such as the intestine or visceral adipose tissue (16). Others suggested that Gremlin-1 plays an important role in visceral adipose tissue biology by driving adipocyte hypertrophy and adipose tissue dysfunction (24). Given the important role of visceral adipose tissue dysfunction in MASLD/MASH development (23), Gremlin-1 could drive the development and progression of MASH by modulating local adipose tissue function. Some authors even have hypothesized that visceral adipose tissue Gremlin-1 might act directly on the liver via delivery through the bloodstream (19), but this seems unlikely considering the high affinity binding of Gremlin-1 to glycosaminoglycans such as heparin, which very likely prevents Gremlin-1 from entering the blood stream. We carefully selected the CDAA-HFD rat model of MASH fibrosis for our *in vivo* studies as this was the only animal model tested that showed convincing and reliable hepatic upregulation of Gremlin-1 upon liver injury. While the CDAA-HFD model reliably reproduces the histological hallmarks of hepatic disease in MASH, such as liver steatosis, inflammation and fibrosis (30), it does not incorporate extrahepatic factors such as obesity and adipose tissue dysfunction as drivers of disease. On the contrary, CDAA-HFD leads to reduced weight gain and reduced visceral adiposity compared to control diet (30). Data on adipose tissue biology in CDAA-HFD are scarce, but increased expression and release of the obesogenic cytokine leptin is considered a hallmark of severe obesity and the metabolic syndrome (31). Experiments on mice suggest that this axis is disrupted in CDAA-fed animals as they show reduced leptin levels (32). Likewise, although not specifically tested, obesity-induced changes in adipose tissue Gremlin-1 expression and biology are likely not reflected in the CDAA-HFD model used here.

Precision-cut liver slices (PCLS) are a well-established method that allows the study of hepatic signalling pathways *ex vivo*, and unlike monolayer cell culture models reflects hepatic cell-cell interactions (33). We used liver specimen from patients

undergoing liver transplantation, which enabled us to study the effects of anti-Gremlin-1 treatment on clinically relevant, chronically diseased liver. However, these samples were derived from patients with end-stage liver disease which is usually not amenable to pharmacological interventions aimed at reversing disease. We were also limited to studying samples after 24 hours of treatment, because we observed tissue and RNA degradation when keeping cirrhotic PCLS in culture for longer. While others have incubated cirrhotic PCLS for up to 48 hours, they still observed significant changes in gene expression as early as 24 hours after dosing (34), and we also found a clear anti-fibrotic response upon ALK5 inhibition, so it is unlikely that the shorter duration of our experiment precluded us from observing early effects of Gremlin-1 blockade . However, any potential effects of Gremlin-1 on infiltrating immune cells and extrahepatic signals, e.g. from the gut or adipose tissue, are not reflected in PCLS.

Our negative findings from rat *in vivo* and human *ex vivo* models were largely corroborated by our results obtained through *in vitro* cell culture of fibrotic liver cells. Anti-Gremlin-1 treatment was ineffective in reducing pro-fibrogenic gene expression in both LX-2 and primary HHSC. This was in line with findings that lentiviral overexpression of GREM1 in both cell types did not alter the expression of fibrogenic genes in response to TGFβ1. Interestingly, overexpression of GREM1 increased the expression of CCL2, a proinflammatory cytokine upregulated in early stellate cell activation (29) and LOX, which plays an important role in collagen-crosslinking and is typically upregulated later in the HSC activation cascade (29,35). GREM1 overexpression also modulated the expression of BMP-signalling-related genes, including BMP7, SMADs and INHBB, which might counter-balance any potential pro-fibrogenic effect.

Overall, considering the minor role of periportal fibroblasts, the main cell population expressing Gremlin-1, in MASH fibrosis and the lack of an effect upon neutralisation of Gremlin-1, the role of hepatic Gremlin-1 in liver fibrosis seems questionable. While some authors described *in vivo* effects of siRNA knockdown of Gremlin-1 on liver fibrosis in a carbon tetrachloride model of liver fibrosis in rats (22), others did not find any effect of adenoviral overexpression or intraperitoneal injection of recombinant Gremlin-1 protein on steatosis, inflammation and fibrosis in high-fat diet-fed mice (36). Furthermore, recent studies suggest that Gremlin-1 might not be a solely pro-fibrotic protein through inhibition of BMPs. Studies on myocardial fibrosis, urinary carcinoma and intervertebral disc degeneration found that Gremlin-1 can also directly antagonise TGFβ1 (37–39), thereby potentially exerting anti-fibrotic effects. Therefore, the specific role of Gremlin-1 in organ fibrosis might be largely context-dependent, depending on the local balance of BMPs and TGF proteins.

Our findings regarding the heparin-binding properties of Gremlin-1 shed further light on biological function and potential use of Gremlin-1 as a biomarker or therapeutic target. Heparin binding is a hallmark of the TGFβ superfamily of proteins (40), including Gremlin-1 belonging to the Dan family, and therefore it was not unexpected that Gremlin-1 also possesses high-affinity binding properties towards glycosaminoglycans such as heparan sulphate (41). To our surprise, using our highly sensitive and specific luminescent channelling assays, we found no consistent evidence of circulating Gremlin-1 protein. Other groups reported increased levels of Gremlin-1 protein in the blood of patients with MASLD/MASH and cardiovascular disease and even found correlations with parameters of hepatic disease activity and insulin resistance (19). Proving the absence of a protein is inherently challenging if not impossible. Still, leading up to this assay we tested many high-affinity polyclonal and monoclonal antibodies, exploiting all epitopes of Gremlin-1 to avoid epitope

masking in circulation. Using these antibodies on several detection platforms, we still found no detectable Gremlin-1 in circulation, despite high-sensitivity of our assays, which was confirmed using spike-ins of recombinant protein from several batches and the presence of detectable Gremlin-1 in circulation after anti-Gremlin-1 treatment in the rat CDAA-HFD model. Furthermore, the absence of any signal suggests that unspecific binding was not an issue. We are therefore confident that our assay worked and that we should have been able to pick up signals from Gremlin-1 concentrations as high as have been reported in the literature. We propose that the heparin-binding properties of Gremlin-1 preclude release of Gremlin-1 protein into systemic circulation while it is retained locally in its functional niche, amplifying local activity surrounding Gremlin-1-expressing cells. However, this likely precludes release of Gremlin-1 protein into systemic circulation. Therefore, previous findings relating to correlations of circulating Gremlin-1 need to be interpreted with caution. Still, extracellular vesicles (42) and platelets (43) reportedly can contain Gremlin-1, which might still offer a route of inter-organ communication through Gremlin-1. Taken together, the implications of Gremlin-1 heparin-binding properties and possibility of its absence from systemic circulation clearly need to be considered when studying its function, therapeutic applications and suitability as a biomarker.

In summary, our data provide compelling evidence that hepatic Gremlin-1 is not a suitable target for treating MASH-induced liver fibrosis. However, this does not preclude a role for Gremlin-1 in other liver diseases, and biliary fibrosis in particular. Furthermore, mounting evidence suggests a role for Gremlin-1 in carcinogenesis and future studies will have to define its role in hepatocellular carcinoma development. Not least, the role of Gremlin-1 in adipose tissue is well established and targeting visceral adipose rather than hepatic Gremlin-1 might be a more promising target in

412 MASH. More research is needed though, to confirm a link between adipose Gremlin-

413 1 and hepatic inflammation and fibrosis.

Materials and Methods

Study approval

All work on human tissue and blood conformed with the Human Tissue Act and studies were approved by the local ethics review board (Immune regulation, 06/Q2702/61 and 04/Q2708/41; Inflammation, 18-WA-0214; Fibrosis, 19-WA-0139). Human blood samples for detection of Gremlin-1 protein were collected as part of the Fatty Liver Disease in Nordic Countries (FLINC) study (Clinicaltrials.gov, NCT04340817, ethics protocol number: H-17029039, approved by Scientific Ethics Committees in The Capital Region of Denmark) and human liver biopsies for ISH staining were obtained in routine clinical practice and use for research was approved by the local ethics committee (ethics protocol number: H-17035700, approved by Scientific Ethics Committees in The Capital Region of Denmark). All patients or their legal representatives gave informed written consent prior to all procedures.

All animal experiments were performed at Novo Nordisk, Denmark and were approved by The Danish Animal Experiments Inspectorate using permission 2017-15-0201-01215.

Animal experiments

Male, 8-10 weeks old Sprague Dawley rats (n=130 Janvier Labs, France) were fed a high fat, choline-deficient, 1% cholesterol diet (CDAA-HFD [A16092003, Research Diets Inc, New Brunswick, New Jersey]) for 12 weeks, with weekly subcutaneous administration of 25, 2.5, 1 or 0.25 mg/kg of NNC0502-2021 heparin-displacing or 25, 2.5, or 1 mg/kg NNC0502-0361 non heparin-displacing antibody during weeks 6 to 12. The first dose was administered as a double dose, to increase time spent at

steady state drug exposure. As a control, isotype mouse IgG1 antibody was administered at 25 mg/kg. A separate group of animals was fed control chow diet (n=5, chow, Altromin 1324, Brogaarden, Lynge, Denmark) for the duration of the study. After 6 weeks dosing, animals were sacrificed in a fed state 6 days post last dose, and plasma and tissue were collected for analysis. Plasma was collected by sublingual sampling two days before drug administration for the first two weeks, as well as two days after drug administration throughout the study duration. Liver enzymes alanine transaminase (ALT) and aspartate aminotransferase (AST) in plasma were quantified according to manufacturer's instructions on the Cobas C501 machine (Roche Diagnostics, Basel, Switzerland).

Human liver samples and ethics

Tissue samples were taken from explanted diseased livers of patients undergoing liver transplantation for end-stage liver disease of different aetiology (MASLD/MASH, alcohol-related liver disease, primary biliary cholangitis, primary sclerosing cholangitis) or donor livers from organ donors that were not deemed suitable for transplantation after organ retrieval.

Generation of human therapeutic anti-Gremlin-1 antibody

The Adimab antibody discovery platform was used to select antibodies against Gremlin-1 as described in the following. Eight separate libraries, representing different antibody families and each with a 1-2 × 10^9 diversity, were screened for specific binders through consecutive rounds of enrichment using MACS and FACS. In short, using biotinylated rhGremlin as a "bait" protein, two rounds of MACS

selections were performed followed by three rounds of FACS, including a de-selection round for poly-specific binders. After the final selection round, clones were plated, picked and sequenced from each of the libraries. From the pool of sequences, unique antibodies were identified, and these were expressed, purified, and subsequently tested for binding to Gremlin-1 using Fortebio technology. To increase the panel of high affinity antibodies, a light chain shuffle was performed using the heavy chain output from the naïve selection. For use in the rat MASH study, the human variable light and heavy chains were grafted onto a murine scaffold.

Cell culture

Primary human HSEC, BEC and myofibroblasts were isolated as described previously (44,45). HSEC and BEC were used for RNA isolation purposes only. Myofibroblasts were grown on uncovered polystyrene culture plates in 16% FCS in DMEM supplemented with 1% Penicillin-Streptomycin-L-Glutamine and subcultured at a 1:3 ratio using Gibco TrypLE^{TM} Express Enzyme (12605010, Fisher Scientific) for cell dissociation. Only myofibroblasts up to a passage number of 4 were used for experiments. For cell culture experiments, myofibroblasts were seeded at a density of $15x10^3$ cells/cm² in 16 % FBS, 1 % Penicillin-Streptomycin-L-Glutamine (10378016, FisherScientific Ltd) in Gibco DMEM (high-glucose, containing pyruvate, 10313021, FisherScientific Ltd) on uncoated polystyrene cell culture multiwell plates. Cells were grown to adhere over 24 hours and serum-starved in 2 % FBS medium (containing Penicillin-Streptomycin-L-Glutamine) for another 24 hours before changing medium to treatment conditions in 2 % FBS medium.

LX-2 cells were purchased from Merck (SCC064, Merck KGaA, Germany), reconstituted and cultured according to the distributor's instructions. Cells were subcultured at a 1:3 to 1:6 ratio using Gibco TrypLE^{TM} Express Enzyme (12605010, Fisher Scientific) for cell dissociation. Only LX-2 cells up to a passage number of 15 were used for experiments. For cell culture experiments, LX-2 cells were seeded at a density of 25x10^3 cells/cm² in 2 % FBS, 1 % Penicillin-Streptomycin-L-Glutamine (10378016, FisherScientific Ltd) in Gibco DMEM (high-glucose, containing pyruvate, 10313021, FisherScientific Ltd) on uncoated polystyrene cell culture multiwell plates. Cells were grown to adhere over 24 hours and serum-starved in 0.2 % FBS medium (containing Penicillin-Streptomycin-L-Glutamine) for another 24 hours before changing medium to treatment conditions in 0.2 % FBS medium.

Primary human hepatic stellate cells (HHSC) isolated from adult healthy donors were purchased from Caltag Medsystems Ltd (IXC-10HU-210, Lot numbers: 300075-7, 300079-1, 300080-1). Cells were grown in 10 % FBS, 1% Penicillin-Streptomycin-L-Glutamine (10378016, FisherScientific Ltd) in DMEM (high-glucose, containing pyruvate, 10313021, FisherScientific) and subcultured in 1:4 ratio using Gibco TrypLE^{TM} Express Enzyme (12605010, Fisher Scientific) for cell dissociation. HHSC were used up to a passage number of 3 (parent cells) or 4 (lentivirally transduced cells). For cell culture experiments, HHSC were seeded at a density of 7.5x10^3 cells/cm² in 10 % FBS, 1 % Penicillin-Streptomycin-L-Glutamine in Gibco DMEM (high-glucose, containing pyruvate, 10313021, FisherScientific) on uncoated polystyrene cell culture multiwell plates. Cells were grown to adhere over 24 hours and serum-starved in 2 % FBS medium (containing Penicillin-Streptomycin-L-Glutamine) for another 24 hours before changing medium to treatment conditions in 2 % FBS medium.

HepG2 cells are a human hepatoma cell line and were purchased from ECACC (#κ5011430). Cells were grown in 10% FCS and 1%PSG in DMEM on uncoated polystyrene cell culture flasks and subcultured in a 1:6 ratio using Gibco TrypLE Express Enzyme.

All cells were grown and maintained in cell culture incubators at 37°C in a 5 % CO_2 atmosphere.

Lentiviral overexpression

We used a replication-deficient recombinant second generation lentivirus for *in vitro* overexpression studies. The coding sequence for Gremlin-1 (Origene, Cat-No RC210835) was inserted into the plasmid pWPI (kindly provided by Roy Bicknell at University of Birmingham), followed by the coding sequence for the enhanced Green Fluorescent Protein (eGFP). This plasmid will be referred to as GREM1-pWPI. The pWPI plasmid including the sequence for eGFP but lacking the GREM1 insert (GFP-pWPI) was used to generate an empty vector control in subsequent experiments (GFP-control). GFP-only control and GREM1 lentiviruses were produced by transfecting HEK293T cells with Lipofectamine 3000 (L3000001, Invitrogen) in OptiMEM (31985070, Gibco) containing 14.4 µg GFP-pWPI or GREM1-pWPI, 8.33 µg psPAX2 - providing the lentiviral replication function - and 2.63 µg pMD2.G - for pseudotyping with the VSV-G, enabling cell entry of the virus into mammalian cells. Supernatants were collected on the two days following transfection and concentrated by density gradient centrifugation on 10% sucrose. The concentrated pseudovirus particles were aliquoted and stored at -80°C.

Human cell lines and primary cells were transduced by incubation with 5 µL of the GREM1 or GFP-control virus per 100,000 cells in full growth media. Lentivirally

transduced LX-2 cells were sub-cultured until confluent before being flow-sorted on the BD FACSAriaTM (BD Biosciences) to obtain cells with top 10 % highest eGFP expression. No sorting was performed on primary HHSC due to limitations in cell numbers and long-term culture.

LX-2 pSMAD1 validation assay

The human HSC cell line (LX-2) was used as in vitro bioassay to validate the inhibitory effect of anti-Gremlin antibodies on Gremlin-1 in BMP4 treated cells. Recombinant human BMP4-induced pSMAD1 signalling was measured by AlphaLISA SureFire Ultra p-SMAD1 (Ser463/465) assay kit (Perkin Elmer). To perform the assay, 30.000 cells were seeded in Fibronectin-coated 96 well plates (Nucleon Delta 96 well, Thermo Scientific #167008) and incubated at 37°C and 5% CO_2 overnight. The following day, anti-Gremlin antibody was serially diluted and pre-incubated with 30 nM Gremlin-1 (recombinant human, in-house produced) in assay medium (DMEM without Phenol Red + 0.2 % FBS) for 30 min at room temperature on a plate shaker at 350 RPM. Thereafter, the anti-Gremlin/Gremlin-1 mixes were pre-incubated with 0.1 nM BMP-4 (recombinant human, R&D, #314-BP/CF) for 10 min at room temperature on a plate shaker at 350 RPM. The culture medium of each well in the cell plates was then discarded and replaced with 100 µL anti-Gremlin/Gremlin-1/BMP-4 mixes in duplicates and the cell plates were subsequently incubated for 60 minutes at 37°C and 5% CO_2. After incubation, assay media was removed, and lysis buffer added to perform assay according to pSMAD1 assay protocol from Perkin Elmer. Phospho-SMAD1 activity was quantified on an EnVision® 2105 multimode plate reader using standard AlphaLisa settings. Dose-

response curves were fit using a four-parameter logistic regression and potencies were defined as the EC50s of these fits.

C2C12/BRE-Luc reporter gene assay

To assess the inhibitory effect of anti-Gremlin antibodies on Gremlin-1, we generated a mammalian reporter cell line responsive to BMP-4. C2C12, a mouse myoblast cell line with endogenous expression of BMP receptors, was modified to stably express a BMP responsive element coupled to luciferase.

A BRE-MLP-Luc plasmid was constructed as described by Korchynskyi & Dijke (46) with the exception that the reporter was inserted into a pGL4.20 vector (Promega). For generating the cell line, 1 x10^6 C2C12 cells (ATCC® CRL-1772™) were seeded in 5 mL growth medium (high glucose Dulbecco's Modified Eagle's Medium (Gibco), 20% fetal bovine serum (Gibco) and 1% Penicillin-Streptomycin mix (Gibco)) in a T25 culture flask (Nunc) and incubated at 37°C and 5% CO_2. The following day, a mixture of 1.25 mL OptiMEM (Gibco), 25 µL Lipofectamine 2000 (Invitrogen) and 10 µg BRE-MLP-Luc plasmid was added to the culture flask. On day 3, puromycin (Gibco) was added to the flask for a final concentration of 2 µg/mL to select for cells which had stably incorporated the transfected plasmid. The cells were cultured in growth medium with a supplement of 2 µg/mL puromycin until confluent, then a single cell clone was isolated. The resulting stable clone, C2C12/BRE-Luc, would emit luminescence following stimulation with BMP-4 in a concentration dependent manner upon addition of luciferase substrate.

The C2C12/BRE-Luc cell line was maintained in high glucose Dulbecco's Modified Eagle's Medium, 20% fetal bovine serum, 1% penicillin-streptomycin mix and 2 µg/mL puromycin. To perform the assay, 6,000 C2C12/BRE-Luc cells were seeded

per well in 384 well tissue culture coated plates (Greiner) and incubated at 37°C and 5% CO_2 overnight. The following day, serial dilutions of therapeutic anti-Gremlin antibody (in-house) were prepared and pre-incubated with recombinant human Gremlin-1 (in-house) for 20 min at room temperature on a plate shaker at 350 RPM. Thereafter, the anti-Gremlin/Gremlin-1 mixes were incubated with recombinant human BMP-4 (R&D, #314-BP/CF) for 20 min at room temperature on a plate shaker at 350 RPM. All dilutions were performed in high glucose Dulbecco's Modified Eagle's Medium with 1% penicillin-streptomycin, resulting in final concentrations of anti-Gremlin, Gremlin-1 and BMP-4 of 100-0.78 nM, 50 nM and 1 nM, respectively. Subsequently, culture medium was replaced with 25 µL anti-Gremlin/Gremlin-1/BMP-4 mixes in duplicates and culture plates were incubated for 6 hours at 37°C and 5% CO_2. Luminescence was detected following addition of 25 µL luciferase substrate (Steady-GLO, Promega). Dose-response curves were fitted using a four-parameter logistic regression and potencies were defined as the EC50s of these fits. Efficacies were defined as the maximal amount of inhibition relative to a positive control, where no Gremlin-1 was added, in percent.

Gremlin-1/BMP-4 inhibition ELISA

Inhibitory potential of anti-Gremlin towards Gremlin-1 binding to BMP-4 was investigated in an enzyme linked immunosorbent assay (ELISA). 384 well Maxisorp plates (Nunc) were coated with 25 µL 2 µg/mL recombinant human BMP-4 (R&D, #314-BP/CF) in 0.1 M, pH 9.6 carbonate buffer and incubated at 4°C overnight. The following day, plates were washed with phosphate buffered saline (PBS) with 0.5% Tween-20 and blocked by incubating with 1% bovine serum albumin in PBS for 4 hours at room temperature on a plate shaker at 350 RPM. Meanwhile, anti-Gremlin

antibody was serially diluted and pre-incubated with primary amine biotinylated (degree of labelling ≈ 1) recombinant human Gremlin-1 (in-house) for 20 min at room temperature on a plate shaker at 350 RPM. Dilutions were performed with phosphate buffered saline with 0.2% Tween-20 and the final concentrations of anti-Gremlin antibody and biotinylated Gremlin-1 were 40-0.09 nM and 10 nM, respectively. After blocking, plates were washed as described above, and 25 µL per well anti-Gremlin/biotin-Gremlin-1 mixes were added and incubated for 1 hour at room temperature on a plate shaker at 350 RPM. To detect plate-bound biotinylated Gremlin-1, plates were washed, as described above, and 25 µL per well 0.06 µg/mL streptavidin horseradish peroxidase conjugate (Thermo Scientific) was added. After 15 min incubation at room temperature on a plate shaker at 350 RPM, plates were washed, as described above, and 25 µL per well horseradish peroxidase substrate (TMB ONE ECO-TEK, Kementec) was added. The reaction was stopped after 5 min incubation by adding 25 µL per well 10% phosphoric acid and Gremlin-1 binding to BMP-4 was quantified by detecting absorbance at 450 nm subtracted by absorbance at 620 nm. Dose-response curves were fitted using a four-parameter logistic regression and potencies were defined as the IC50s of these fits. Efficacies were defined as the maximal amount of inhibition relative to the background signal, where no biotin-Gremlin-1 was added, in percent.

Fluorescence polarization assay

The binding affinity of Gremlin-1 or Gremlin-1-mAb mixtures to fluorescein-labelled Heparin (Heparin-FL, H7482, Thermo Fisher Scientific) was measured in a fluorescence polarization assay. A 12-point dilution series of Gremlin-1 or Gremlin-1/mAb was titrated to a constant Heparin-FL concentration of 10 nM in 20 mM

HEPES, 150 mM NaCl, 0.05% (v/v) polysorbate 20, pH 7.4. The highest Gremlin-1 concentration assayed was thus 1 µM, referring to the dimer. In mAb-containing samples, mAb was used at a 1.5x molar excess, i.e. 1.5 µM at the highest concentration, and diluted alongside Gremlin-1 (so that the 1.5x molar excess was maintained throughout the dilution series). Both tested mAbs bind to Gremlin with high affinity (K_D < 1 nM), so the mAb-Gremlin-1 complex can be assumed to be the dominating species in the mixture over the whole concentration range tested. Samples were incubated for 5 h at room temperature and fluorescence polarization was measured in duplicate in a 384-well plate (Cat # 784900, Greiner) on a microplate reader (Spark, Tecan), using 485/20 nm and 535/25 nm excitation and emission filters, respectively (a second measurement after 20 h confirmed that equilibrium was reached in the 5 h measurement). The binding curve was fitted with a 1:1 binding isotherm in GraphPad Prism (Graph Pad software), using the equation $S = a\frac{x}{K_D+x} + b$, with S the measured fluorescence polarization, b the fluorescence polarization signal of the unbound Heparin-FL, a the amplitude of the signal change, x the Gremlin-1 concentration and K_D the binding affinity. The K_D obtained thus is an upper limit, as first order conditions are not given in the case of free Gremlin, which binds with a K_D close to the Heparin-FL tracer concentration. However, the observed trend is robust towards this treatment. The parameters a and b were shared among the fits to increase robustness of the fitting procedure.

SEC-MALS for complex formation between Gremlin-1, Heparin and mAbs

To characterize complexes formed between Gremlin-1 and mAbs, samples were prepared at 5.5 µM of Gremlin-1 (referring to the dimer) and 5.5 µM of respective mAb in in 20 mM HEPES pH 7.5, 500 mM NaCl. To assess complex formation

between Gremlin-1 and Heparin, a sample was prepared at 2.75 µM Gremlin-1 concentration (referring to the dimer) and 2.75 µM Heparin (Applichem 3004,0001) in 20 mM HEPES pH 7.5, 300 mM NaCl. To assess complex formation between Gremlin-1, Heparin, and mAb, samples were prepared at 2.75 µM Gremlin-1 concentration (referring to the dimer), 2.75 µM Heparin, and 2.75 µM of respective mAb in 20 mM HEPES pH 7.5, 300 mM NaCl. All samples were incubated for at least 2 h at 7ºC before injection. 50 µL of sample were injected on a HPLC system (Alliance, Waters) and separated on a Superose 6 increase 10/300 GL column (GE Healthcare) equilibrated with 20 mM HEPES pH 7.5, 300 mM NaCl (flow: 0.5 ml/min). To analyse the mAb-Gremlin-1 complexes, a running buffer containing 20 mM HEPES pH 7.5, 500 mM NaCl was used instead. Eluting sample was detected with light scattering (miniDAWN Treos, Wyatt), RI (Optilab rEX, Wyatt) and UV detectors. The light scattering data was analysed in Astra (Wyatt), assuming a refractive index increment of 0.185 mL/g for all analyses.

Gremlin-1 cell association assay

Association of Gremlin-1 to cells in culture and the ability of anti-Gremlin to prevent this association was assessed with confocal microscopy.

To prepare fluorescently labelled Gremlin-1, 30 nmol of the protein monomer was incubated with 20 nmol of Atto 532-NHS ester (ATTO-TEC) for 2.5 h in the dark at room temperature, in 20 mM HEPES, 500 mM NaCl, pH 7.5 as the labelling buffer. The Gremlin-1 monomer concentration in the reaction was kept at 250 µM. The fluorescent dye stock was prepared at 9.25 mM in DMSO. After the reaction was completed, free dye was removed by buffer exchange into labelling buffer, using Zeba spin desalting columns (7K MWCO, 0.5 mL, Thermo Fisher Scientific),

according to the manufacturers' protocol. The degree of labelling was determined by UV/Vis spectroscopy to 0.56 dye molecules/Gremlin-1 monomer.

15,000 LX-2 cells per well were seeded in growth medium (high glucose Dulbecco's Modified Eagle's Medium, 2% fetal bovine serum and 1% penicillin-streptomycin mix) in a microscopy microtiter plate (CellCarrier-96 ultra, PerkinElmer). On the following day, sample solutions with 250 nM Atto-532-labelled (degree of labelling ≈ 1) Gremlin-1 (recombinant human, in-house) and 1 mg/mL anti-Gremlin, 1 mg/mL unrelated human IgG1.1 isotype control (recombinant human, in-house) or no antibody were prepared in growth medium. Wells were emptied, 50 µL/well sample solutions were added, and the plate was incubated for 24 hours at 37°C and 5% CO_2. Following incubation, well contents were removed, and the cells were washed three times with 100 µL/well PBS. Thereafter, cells were fixed by incubation with 100 µL/well 4% PBS-buffered paraformaldehyde for 15 min at room temperature. The cells were washed, as described above, and permeabilized by incubation with 100 µL/well 0.1% Triton X-100 in PBS for 15 min at room temperature. The cells were washed, as described above, and 100 µL/well cell staining solution (1:5,000 HCS CellMask Blue, Thermofisher in PBS) was added followed by a 30 min incubation at room temperature in the dark. The cells were washed, as described above, and 100 µL/well PBS was added. Immediately thereafter, the cells were imaged confocally in blue and orange channels on a High Content Imaging System (Operetta CLS, PerkinElmer).

Human precision-cut liver slices

To study the effects of interventions targeted at Gremlin-1 in a human *ex vivo* model of liver fibrosis, we used the method of precision-cut liver slices (PCLS). Cylinders of

liver tissue were prepared by taking biopsies from explant livers using an 8 mm skin biopsy blade. Next, we embedded these cylinders in 3 % low-melt Agarose (A9414, Sigma) in phenol-free Hank's Buffered Salt Solution (HBSS, 14175095, Gibco) and cut 250 µm thick sections using a vibratome (VT1200S, Leica biosystems). The slices were then equilibrated in pre-warmed full PCLS culture medium (Williams E medium + 2 % FBS + 1 % penicillin-streptomycin-L-glutamine + 1x insulin-transferrin-selenium + 100 nM dexamethasone) at 37°C for one hour, and in the meanwhile, treatment conditions were prepared in PCLS culture medium. Treatment solutions were then added at 1.5 mL per well into 3 µm transwell inserts in a 12-well plate (GD665631, SLS). Finally, one piece of PCLS was transferred into each respective transwell and the plates were incubated for 24 h on an orbital rocker at 20 rpm, 37°C in a humidified 5% CO_2 atmosphere. At the end of the incubation period, liver slices were collected, snap-frozen in liquid N_2 and stored at -80°C until further processing. Supernatants were collected, and spun down at 10,000xg for 10 min to remove cellular debris, snap-frozen in liquid N_2 and stored at 80°C until further processing.

Luminescent oxygen channelling immunoassay

Luminescent Oxygen Channeling assays (LOCI) were based on anti-gremlin monoclonal antibody pairs generated at Novo Nordisk A/S, Denmark. Acceptor beads (6772004L, PerkinElmer) were directly coupled to antibodies while -streptavidin coated donor beads (6760002L, Perkin Elmer) were a used in combination with biotinylated antibodies. Recombinant human gremlin protein, Novo Nordisk A/S, China, was used as calibrator material and positive control. Briefly, a mixture of the conjugated acceptor beads and the biotinylated antibodies were produced to a final concentration of 33.3 µg/ml and 0.75 µg/ml, respectively. In a 384 well assay plate,

735 15 µl of the mixture were added to 5 µl of plasma sample and incubated for 1 hour at
736 room temperature (RT) in the dark. Next, 30 µl of donor beads (67 µg/ml) were added
737 to each sample and the plate was incubated for 30min at RT. Addition of donor
738 beads were done in a green-light room to avoid bleaching. The samples were
739 analysed on a PerkinElmer Envision instrument. All samples were measured in
740 duplicates.

741 ***Immunohistochemistry***

742 Rat liver samples (full-thickness slabs of left lateral lobes) were fixed 3-5 days in
743 neutral-buffered formalin (NBF). Liver tissue was routine paraffin-embedded and
744 sectioned (4 µm nominal thickness). Sections were stained manually with Picro Sirius
745 Red (PSR), and in the Ventana Autostainer with anti-CD45 at 2 µg/ml (Abcam
746 ab10558, Cambridge, UK), anti-alpha-smooth muscle actin (α-SMA) at 0.04 µg/ml
747 (clone EPR5368, Abcam ab124964), anti-CD68 at 1.5 µg/ml (clone E3O7V, Cell
748 Signaling 97778, Danvers, MA), anti-CD11b at 0.5 µg/ml (clone EPR1344, Abcam
749 ab133357), or anti-type I collagen at 4 µg/ml (Southern Biotech 1310-01,
750 Birmingham, AL) using heat-induced epitope retrieval at basic pH, HRP-coupled
751 detection polymers, and the Purple chromogen. All primary antibodies were of rabbit
752 or goat origin to avoid background from the mouse anti-gremlin therapeutic antibody.
753 Stained liver sections were scanned as 8-bit RGB colour images (pixel size: 442 nm)
754 using a NanoZoomer S60 digital slide scanner (Hamamatsu Photonics K.K.,
755 Hamamatsu City, Japan). Quantitative image analysis was applied to the entire liver
756 sections using Visiopharm Integrator System software (VIS ver. 8.4; Visiopharm,
757 Hørsholm, Denmark). The fractional area (%) of PSR, steatosis, CD45, α-SMA,
758 CD68, CD11b, and Col1a1 stains was expressed relative to total sectional area.

759

RNAscope in situ hybridization

Twenty-five human diagnostic, formalin-fixed, paraffin-embedded (FFPE) histological liver needle biopsies were retrieved from the archives at Department of Pathology at Aalborg University Hospital, Denmark. The biopsies were diagnosed as normal, n=5, non-alcoholic steatohepatitis (MASH) with mild fibrosis, n=7, MASH with moderate/severe fibrosis, n=6, and MASH with cirrhosis, n=7. RNAscope duplex in situ hybridization (ISH) was performed on the Leica Biosystems BOND RX platform. RNAscope probes (Advanced Cell Diagnostics (ACD) Newark, California) directed against human GREM1 and human THY1 or COL3A1 were hybridized for 2 h at 42°C using RNAscope 2.5 LS Duplex Reagent Kit (ACD) followed by RNAscope amplification. Fast red chromogenic detection of GREM1 was followed by green chromogenic detection (ACD) of THY1 or COL3A1. Sections were counterstained with haematoxylin. The GREM1-positive dot area fraction (dot area per tissue area) of single RNAscope ISH with the GREM1 probe has been quantified using HALO v3.5.3577 and the Area Quantification v2.4.2 module.

RNA isolation and reverse transcription

RNA from cells was isolated using the RNeasy Mini Kit or RNeasy Micro Kit (74104 and 74004, respectively, QIAgen, Germany), following manufacturer's instructions, including on-column DNA digestion (RNase-Free DNase Set, 79254, QIAGEN). RNA from human liver tissue and human cirrhotic PCLS was isolated using Tri Reagent (T9424, Sigma) and 1-bromo-3-chloropropane (B9673, Sigma) according to manufacturer's instructions. Following Tri Reagent extraction, RNA clean-up was performed using the RNeasy Mini Kit according to the manufacturer's instructions, including on-column DNA digestion.

RNA from rat liver tissue was snap frozen in RNAlater and lysed using lysis buffer (RNAdvanced Kit, A32646, Beckman Coulter), 20µL Proteinase K on a TissueLyser II (Qiagen) for 2 min at 25 Hz and 3 min at 30 Hz. After adding additional 350 µL of lysis buffer, samples were incubated at 37°C for 25 min. RNA was then isolated using Agencourt RNAdvanced Tissue Kit on a Biomeki7 (Beckman Coulter), including DNase treatment (RNAse-free DNase1, Quiagen), according to manufacturer's instructions.

RNA concentrations were determined on a spectrophotometer (NanoPhotometer Classic, Implen, or NanoDrop 8000, Thermo Scientific) and reverse-transcribed to cDNA with the High-capacity cDNA Reverse Transcription Kit (4368813, Applied Biosystems) or iScript Supermix reverse transcriptase (#1708841, BioRad) according to manufacturer's instructions.

Quantitative PCR

Gene expression on human cells and tissue was quantified using TaqMan™ assays (Fisher Scientific, Supplementary Table 3) and Luna® Universal qPCR Master Mix (M3003E, New England BioLabs) on a LightCycler 480 II (Roche Diagnostics) according to manufacturer's instructions. Gene expression was normalized to the expression of SRSF4 or a combination of SRSF4, HRPT1, ERCC3 and CTCF for cell culture or liver tissue expression, respectively.

Gene expression on rat liver was quantified using TaqMan™ assays (Fisher Scientific, Supplementary Table 3) and TaqMan fast advanced mastermix (Thermo #4444964, Thermo Fisher Scientific) on a QuantStudio 7 Real-Time PCR system (Thermo Fisher Scientific) according to manufacturer's instructions. Gene expression was normalised to peptidylpropyl isomerase B (*PPIB*) mRNA levels.

Expression of GREM1, eGFP and GAPDH mRNA in lentivirally transduced cells was quantified using custom-made primers (Sigma, Supplementary Table 4) and PowerUp™ SYBR™ Green Master Mix (A25741, Applied Biosystems) on a LightCycler 480 II. Gene expression was normalized to the expression of GAPDH.

RNA sequencing

RNA was isolated as described above and quality checked on a spectrophotometer. RNA was then submitted to Genomics Birmingham at the University of Birmingham for further quality control, library preparation and sequencing. Quality control was performed using Qubit High Sensitivity RNA assay (Q32852, Invitrogen™) on a Qubit 2.0 fluorometer (Invitrogen) and RNA ScreenTape (5067-5576, Agilent) on the Agilent TapeStation 4200. Single-end 75 base-pair libraries were generated using the QuantSeq 3' mRNA-Seq Library Prep Kit FWD for Illumina (015.96, Lexogen) with an RNA input of 100 ng. Quality of libraries was then checked using the Agilent TapeStation D1000 ScreenTape (5067-5582, Agilent) and Qubit dsDNA High Sensitivity kit (Q32851, Invitrogen). Finally, pooled libraries at 1.6 pM were sequenced on the NextSeq 500 sequencing platform (Illumina) on a NextSeq Mid 150 flowcell.

Raw sequencing files were obtained from Genomics Birmingham at the University of Birmingham. Adapter and quality trimming were performed using fastp using the adapter sequence GATCGGAAGAGCACACGTCTGAACTCCAGTCAC and settings

--trim_poly_g --trim_poly_x --cut_tail --cut_window_size=4 --cut_mean_quality=20

--disable_quality_filtering --low_complexity_filter --complexity_threshold=30

--length_required 36.

After quality control with fastqc, gene abundance was quantified using a decoy-aware transcriptome index (transcriptome gencode version 29, genome GRCh38) and salmon 1.5.9 with default settings. Downstream data import into R and differential gene expression analysis were performed as described for publicly available RNAseq data using the tximport and DESeq2 packages.

Analyses of publicly available transcriptome datasets

Publicly available datasets from liver tissue transcriptome experiments were retrieved from the Gene Expression Omnibus (GEO), the European Nucleotide Archive and ArrayExpress (47–49).

Raw sequencing data were transferred to the public Galaxy server usegalaxy.org to pre-process the data (50). Data were transformed to standard FASTQ format using the fasterq-dump function. Quality control, quality and adapter trimming were performed with fastp and default settings (51). The trimmed sequencing files were then aligned to the human Gencode reference transcriptome (version 36, available from https://www.gencodegenes.org/human) using salmon quant from the pseudoalignment tool salmon with --validate Mappings, --seqBias and --gcBias turned on with default settings (52). For downstream analyses, gene or transcript counts were imported into R using the tximport pipeline for salmon output (53). Differential gene expression was performed with the DESEq2 package using the likelihood ratio test or the Wald test as appropriate (54). Variance stabilised expression values, obtained using the vst function in DESeq2, were used for visualisation of gene expression.

Raw count matrices for liver single-cell RNA sequencing datasets were obtained from the GEO server (GSE136103, (26)) and the Liver Cell Atlas website (GSE192742, (27,55)).

Low quality cells were removed if the number of detected features was below 300 or the percentage of mitochondrial genes per cell was higher than 30 percent. Following quality filtering, gene expression was normalised by cluster-based log-normalisation using the igraph method in the quickCluster function from the scran package (56). Variable features were identified using the fitted mean-variance calculated with the modelGeneVar function with default settings. Doublet contamination was removed using the default method of the doubletFinder v3 package (57).

Following quality control and cleaning of both datasets separately, both datasets were integrated based on their common genes and using the reciprocal principal component analysis (RPCA) method implemented in the Seurat v4 package (58). Based on the integrated gene expression matrix, data scaling, principal component analysis and nearest neighbour graph-based clustering were performed using the standard Seurat workflow. Cell types were manually annotated by marker gene expression obtained from the FindConservedMarkers function in Seurat v4 and based on the annotation provided by the Guilliams lab (27).

Data availability

RNA sequencing data have been deposited in the Gene Expression Omnibus under accession number GSE245977.
https://www.ncbi.nlm.nih.gov/geo/query/acc.cgi?acc=GSE245977

Statistical analysis

All statistical analyses were performed R version 4.2 and using the *rstatix* or *PMCMRplus* package. Graphs were drawn using *ggplot2*, *ggpubr* and *ggprism* packages. Data are shown as means ± SD, if not stated otherwise. Normal distribution was tested by inspecting QQ plots and by Shapiro-Wilks test. To test for homogeneity of variance we used Levene procedure. Depending on data distribution, we used the following statistical procedures: One-way analysis of variance (ANOVA), Two-way ANOVA, Welch's test or Kruskall-Wallis test with post-hoc Bonferroni-Holm, Dunnett, Dunnett-T3 or Dunn-Holm correction and for testing of ordinal or nominal data the χ^2-test. Four parameter log-logistic regression analysis for dose-response experiments was performed using the *drc* package and LL.4 starter function in R. An alternative hypothesis was accepted if two-sided $p < 0.05$.

Author contributions

PH, CJW, MFT and PNN drafted and wrote the manuscript. JN, KA, BMV, AH, FZ, HD, SP, PLN, MGR, MRR, ES, EN and PFL developed assays. PH, JN, KA, BMV, AH, FZ, HD, SP, PLN and MGR performed experiments. EDG and MV procured and interpreted clinical data and liver biopsy specimen. PH, JN, KA, BMV, AH, FZ, HD, SP, PLN, PFL, CJW, MFT and PNN analysed and interpreted the data. PH performed bioinformatics analyses of NGS data. All authors critically revised the manuscript and approved the final version.

Acknowledgements

PH, CJW and PNN were supported by the Birmingham NIHR Biomedical Research Centre. This paper presents independent research supported in part by National institute for Health Research (NIHR) Birmingham Biomedical Research Centre at the University Hospitals Birmingham NHS foundation Trust and the University of Birmingham. (Grant reference number: BRC-1215-20009). The views expressed are those of author(s) and not necessarily those of NIHR or the department of Health and Social care. PH is participant in the BIH Charité Digital Clinician Scientist Program funded by the DFG, the Charité – Universitätsmedizin Berlin, and the Berlin Institute of Health at Charité (BIH).

The authors would like to acknowledge the Genomics Birmingham and Flow Cytometry facilities at the University of Birmingham for support of RNA sequencing experiments and flow sorting lentivirally transduced cells. The authors would like to acknowledge Celina Whalley, Charlie Poxon and Adriana Flores-Langarica.

We also want to thank Emma Collins, Jeanette Juul, Helene Lykkegaard, Jette Mandelbaum, Malik N. Nielsen, Casper M. Poulsen, Pia Rothe and Marie Louise Therkelsen for their contribution to data generation and excellent technical assistance.

Conflict of interest

PH, PFL and CJW report research funding from Novo Nordisk through the University of Birmingham.

JN, KA, BMV, EDG, AH, FZ, HD, SP, PLN, MGR, MFT are full-time employees of Novo Nordisk A/S.

926 PNN reports consulting for Boehringer Ingelheim, Novo Nordisk, Intercept, Gilead,
927 Poxel Pharmaceuticals and BMS on behalf of the University of Birmingham and
928 research grants from Novo Nordisk and Boehringer Ingelheim.

929 MV, MRR, ES, and EN report no conflicts of interest related to this manuscript.

930

References

1. Younossi ZM, Koenig AB, Abdelatif D, Fazel Y, Henry L, Wymer M. Global epidemiology of nonalcoholic fatty liver disease—Meta-analytic assessment of prevalence, incidence, and outcomes. Hepatology. 2016;64(1):73–84.

2. Younossi Z, Anstee QM, Marietti M, Hardy T, Henry L, Eslam M, et al. Global burden of NAFLD and NASH: Trends, predictions, risk factors and prevention. Nat Rev Gastroenterol Hepatol. 2018;15(1):11–20.

3. Powell EE, Wong VWS, Rinella M. Non-alcoholic fatty liver disease. The Lancet. 2021 Jun 5;397(10290):2212–24.

4. Taylor RS, Taylor RJ, Bayliss S, Hagström H, Nasr P, Schattenberg JM, et al. Association between fibrosis stage and outcomes of patients with nonalcoholic fatty liver disease: A systematic review and meta-analysis. Gastroenterology. 2020 Feb;158(6):1611-1625.e12.

5. Church RH, Ali I, Tate M, Lavin D, Krishnakumar A, Kok HM, et al. Gremlin1 plays a key role in kidney development and renal fibrosis. Am J Physiol - Ren Physiol. 2017;312(6):F1141–57.

6. Koli K, Myllärniemi M, Vuorinen K, Salmenkivi K, Ryynänen MJ, Kinnula VL, et al. Bone morphogenetic protein-4 inhibitor Gremlin is overexpressed in idiopathic pulmonary fibrosis. Am J Pathol. 2006 Jul;169(1):61–71.

7. Staloch D, Gao X, Liu K, Xu M, Feng X, Aronson JF, et al. Gremlin is a key pro-fibrogenic factor in chronic pancreatitis. J Mol Med. 2015;93(10):1085–93.

8. Duffy L, Henderson J, Brown M, Pryzborski S, Fullard N, Summa L, et al. Bone Morphogenetic Protein Antagonist Gremlin-1 Increases Myofibroblast Transition in Dermal Fibroblasts: Implications for Systemic Sclerosis. Front Cell Dev Biol [Internet]. 2021;9. Available from: https://www.frontiersin.org/articles/10.3389/fcell.2021.681061/full

9. Topol LZ, Bardot B, Zhang Q, Resau J, Huillard E, Marx M, et al. Biosynthesis, post-translation modification, and functional characterization of Drm/Gremlin. J Biol Chem. 2000;275(12):8785–93.

10. Mitola S, Ravelli C, Moroni E, Salvi V, Leali D, Ballmer-Hofer K, et al. Gremlin is a novel agonist of the major proangiogenic receptor VEGFR2. Blood. 2010;116(18):3677–80.

11. Mueller KAL, Tavlaki E, Schneider M, Jorbenadze R, Geisler T, Kandolf R, et al. Gremlin-1 identifies fibrosis and predicts adverse outcome in patients with heart failure undergoing endomyocardial biopsy. J Card Fail. 2013 Oct;19(10):678–84.

12. Grillo E, Ravelli C, Corsini M, Ballmer-Hofer K, Zammataro L, Oreste P, et al. Monomeric gremlin is a novel vascular endothelial growth factor receptor-2 antagonist. Oncotarget. 2016;7(23):35353–68.

13. Tatsinkam AJ, Rune N, Smith J, Norman JT, Mulloy B, Rider CC. The binding of the bone morphogenetic protein antagonist gremlin to kidney heparan sulfate:

971 Such binding is not essential for BMP antagonism. Int J Biochem Cell Biol.
972 2017;83:39–46.

973 14. Kišonaite M, Wang X, Hyvönen M. Structure of Gremlin-1 and analysis of its
974 interaction with BMP-2. Biochem J. 2016;473(11):1593–604.

975 15. Tatsinkam A, Mulloy B, Rider CC. Mapping the heparin-binding site of the BMP
976 antagonist gremlin by site-directed mutagenesis based on predictive modelling.
977 Biochem J. 2015;470(1):53–64.

978 16. Gustafson B, Hammarstedt A, Hedjazifar S, Hoffmann JM, Svensson PA,
979 Grimsby J, et al. BMP4 and BMP antagonists regulate human white and beige
980 adipogenesis. Diabetes. 2015 May;64(5):1670–81.

981 17. Boers W, Aarrass S, Linthorst C, Pinzani M, Elferink RO, Bosma P.
982 Transcriptional profiling reveals novel markers of liver fibrogenesis: Gremlin and
983 insulin-like growth factor-binding proteins. J Biol Chem. 2006;281(24):16289–95.

984 18. Ogawa T, Tateno C, Asahina K, Fujii H, Kawada N, Obara M, et al. Identification
985 of vitamin A-free cells in a stellate cell-enriched fraction of normal rat liver as
986 myofibroblasts. Histochem Cell Biol. 2007;127(2):161–74.

987 19. Hedjazifar S, Shahidi RK, Hammarstedt A, Bonnet L, Church C, Boucher J, et al.
988 The novel adipokine gremlin 1 antagonizes insulin action and is increased in type
989 2 diabetes and NAFLD/NASH. Diabetes. 2020 Mar;69(3):331–41.

990 20. Baboota RK, Rawshani A, Bonnet L, Li X, Yang H, Mardinoglu A, et al. BMP4 and
991 Gremlin 1 regulate hepatic cell senescence during clinical progression of
992 NAFLD/NASH. Nat Metab. 2022 Aug;4(8):1007–21.

993 21. Zhang YQ, Wan LY, He XM, Ni YR, Wang C, Liu CB, et al. Gremlin1 accelerates
994 hepatic stellate cell activation through upregulation of TGF-Beta expression. DNA
995 Cell Biol. 2017 Jul;36(7):603–10.

996 22. Zeng XY, Zhang YQ, He XM, Wan LY, Wang H, Ni YR, et al. Suppression of
997 hepatic stellate cell activation through downregulation of gremlin1 expression by
998 the miR-23b/27b cluster. Oncotarget. 2016 Dec;7(52):86198–210.

999 23. Gastaldelli A, Cusi K. From NASH to diabetes and from diabetes to NASH:
1000 Mechanisms and treatment options. JHEP Rep. 2019 Oct 1;1(4):312–28.

1001 24. Grillo E, Ravelli C, Colleluori G, D'Agostino F, Domenichini M, Giordano A, et al.
1002 Role of gremlin-1 in the pathophysiology of the adipose tissues. Cytokine Growth
1003 Factor Rev. 2023 Feb 1;69:51–60.

1004 25. Iwaisako K, Jiang C, Zhang M, Cong M, Moore-Morris TJ, Park TJ, et al. Origin of
1005 myofibroblasts in the fibrotic liver in mice. Proc Natl Acad Sci U S A.
1006 2014;111(32):E3297-305.

1007 26. Ramachandran P, Dobie R, Wilson-Kanamori JR, Dora EF, Henderson BEP, Luu
1008 NT, et al. Resolving the fibrotic niche of human liver cirrhosis at single-cell level.
1009 Nature. 2019;575(7783):512–8.

27. Guilliams M, Bonnardel J, Haest B, Vanderborght B, Wagner C, Remmerie A, et al. Spatial proteogenomics reveals distinct and evolutionarily conserved hepatic macrophage niches. Cell. 2022 Jan 20;185(2):379-396.e38.

28. Nishio T, Koyama Y, Fuji H, Ishizuka K, Iwaisako K, Taura K, et al. The Role of Mesothelin in Activation of Portal Fibroblasts in Cholestatic Liver Injury. Biology. 2022 Nov;11(11):1589.

29. Yang W, He H, Wang T, Su N, Zhang F, Jiang K, et al. Single-Cell Transcriptomic Analysis Reveals a Hepatic Stellate Cell-Activation Roadmap and Myofibroblast Origin During Liver Fibrosis in Mice. Hepatol Baltim Md. 2021 Nov;74(5):2774–90.

30. Lefere S, Puengel T, Hundertmark J, Penners C, Frank AK, Guillot A, et al. Differential effects of selective- and pan-PPAR agonists on experimental steatohepatitis and hepatic macrophages☆. J Hepatol. 2020 Oct 1;73(4):757–70.

31. Tilg H, Moschen AR. Adipocytokines: mediators linking adipose tissue, inflammation and immunity. Nat Rev Immunol. 2006 Oct;6(10):772–83.

32. Yang A, Yan X, Fan X, Shi Y, Huang T, Li W, et al. Hepatic stellate cells-specific LOXL1 deficiency abrogates hepatic inflammation, fibrosis, and corrects lipid metabolic abnormalities in non-obese NASH mice. Hepatol Int. 2021 Oct 1;15(5):1122–35.

33. Paish HL, Reed LH, Brown H, Bryan MC, Govaere O, Leslie J, et al. A Bioreactor Technology for Modeling Fibrosis in Human and Rodent Precision-Cut Liver Slices. Hepatology. 2019;70(4):1377–91.

34. Suriguga S, Li M, Luangmonkong T, Boersema M, De Jong KP, Oosterhuis D, et al. Distinct responses between healthy and cirrhotic human livers upon lipopolysaccharide challenge: possible implications for acute-on-chronic liver failure. Am J Physiol-Gastrointest Liver Physiol. 2022 Aug 1;323(2):G114–25.

35. Chen W, Yang A, Jia J, Popov YV, Schuppan D, You H. Lysyl Oxidase (LOX) Family Members: Rationale and Their Potential as Therapeutic Targets for Liver Fibrosis. Hepatology. 2020;72(2):729–41.

36. Shahidi RK, Hoffmann JM, Hedjazifar S, Bonnet L, Baboota RK, Heasman S, et al. Adult mice are unresponsive to AAV8-Gremlin1 gene therapy targeting the liver. PLOS ONE. 2021 Feb 19;16(2):e0247300.

37. Müller II, Schneider M, Müller KAL, Lunov O, Borst O, Simmet T, et al. Protective role of Gremlin-1 in myocardial function. Eur J Clin Invest [Internet]. 2021; Available from: https://pubmed.ncbi.nlm.nih.gov/33729579/

38. Chen S, Lei L, Li Z, Chen F, Huang Y, Jiang G, et al. Grem1 accelerates nucleus pulposus cell apoptosis and intervertebral disc degeneration by inhibiting TGF-β-mediated Smad2/3 phosphorylation. Exp Mol Med. 2022 Apr;54(4):518–30.

39. Chan TC, Pan CT, Hsieh HY, Vejvisithsakul PP, Wei RJ, Yeh BW, et al. The autocrine glycosylated-GREM1 interacts with TGFB1 to suppress TGFβ/BMP/SMAD-mediated EMT partially by inhibiting MYL9 transactivation in

urinary carcinoma. Cell Oncol [Internet]. 2023 Mar 15; Available from: https://doi.org/10.1007/s13402-023-00788-8

40. Rider CC, Mulloy B. Heparin, heparan sulphate and the TGF- Cytokine superfamily. Molecules [Internet]. 2017;22(5). Available from: http://www.ncbi.nlm.nih.gov/pubmed/28468283 https://res.mdpi.com/molecules/molecules-22-00713/article_deploy/molecules-22-00713.pdf?filename=&attachment=1

41. Chiodelli P, Mitola S, Ravelli C, Oreste P, Rusnati M, Presta M. Heparan sulfate proteoglycans mediate the angiogenic activity of the vascular endothelial growth factor receptor-2 agonist gremlin. Arterioscler Thromb Vasc Biol. 2011 Dec;31(12):e116-27.

42. McNamee N, Daly R, Crown J, O'Driscoll L. A method of separating extracellular vesicles from blood shows potential clinical translation, and reveals extracellular vesicle cargo gremlin-1 as a diagnostic biomarker. Transl Oncol. 2022 Jan 1;15(1):101274.

43. Chatterjee M, Behrendt A, Schmid M, Beck S, Schneider M, Mack A, et al. Platelets as a novel source of gremlin-1: Implications for thromboinflammation. Thromb Haemost. 2017;117(2):311–24.

44. Holt AP, Haughton EL, Lalor PF, Filer A, Buckley CD, Adams DH. Liver myofibroblasts regulate infiltration and positioning of lymphocytes in human liver. Gastroenterology. 2009 Feb;136(2):705–14.

45. Edwards S, Lalor PF, Nash GB, Rainger GE, Adams DH. Lymphocyte traffic through sinusoidal endothelial cells is regulated by hepatocytes. Hepatology. 2005;41(3):451–9.

46. Korchynskyi O, Dijke P ten. Identification and Functional Characterization of Distinct Critically Important Bone Morphogenetic Protein-specific Response Elements in the Id1 Promoter *. J Biol Chem. 2002 Feb 15;277(7):4883–91.

47. Barrett T, Wilhite SE, Ledoux P, Evangelista C, Kim IF, Tomashevsky M, et al. NCBI GEO: Archive for functional genomics data sets - Update. Nucleic Acids Res. 2013 Jan;41(D1):D991–5.

48. Harrison PW, Ahamed A, Aslam R, Alako BTF, Burgin J, Buso N, et al. The European Nucleotide Archive in 2020. Nucleic Acids Res. 2021 Jan 8;49(D1):D82–5.

49. Athar A, Füllgrabe A, George N, Iqbal H, Huerta L, Ali A, et al. ArrayExpress update - From bulk to single-cell expression data. Nucleic Acids Res. 2019 Jan;47(D1):D711–5.

50. Afgan E, Baker D, van den Beek M, Blankenberg D, Bouvier D, Čech M, et al. The Galaxy platform for accessible, reproducible and collaborative biomedical analyses: 2016 update. Nucleic Acids Res. 2016 Jul;44(W1):W3–10.

51. Chen S, Zhou Y, Chen Y, Gu J. fastp: an ultra-fast all-in-one FASTQ preprocessor. Bioinformatics. 2018 Sep 1;34(17):i884–90.

52. Patro R, Duggal G, Love MI, Irizarry RA, Kingsford C. Salmon provides fast and bias-aware quantification of transcript expression. Nat Methods. 2017 Mar;14(4):417–9.

53. Soneson C, Love MI, Robinson MD. Differential analyses for RNA-seq: Transcript-level estimates improve gene-level inferences [version 2; referees: 2 approved]. F1000Research. 2016 Feb;4:1521.

54. Love MI, Huber W, Anders S. Moderated estimation of fold change and dispersion for RNA-seq data with DESeq2. Genome Biol. 2014 Dec;15(12):550.

55. Liver Cell Atlas [Internet]. [cited 2023 Jun 19]. Available from: https://www.livercellatlas.org/umap-humanAll.php

56. Lun ATL, McCarthy DJ, Marioni JC. A step-by-step workflow for low-level analysis of single-cell RNA-seq data with Bioconductor. F1000Research [Internet]. 2016;5. Available from: https://pubmed.ncbi.nlm.nih.gov/27909575/

57. McGinnis CS, Murrow LM, Gartner ZJ. DoubletFinder: Doublet Detection in Single-Cell RNA Sequencing Data Using Artificial Nearest Neighbors. Cell Syst. 2019 Apr;8(4):329-337.e4.

58. Hao Y, Hao S, Andersen-Nissen E, Mauck WM, Zheng S, Butler A, et al. Integrated analysis of multimodal single-cell data. Cell. 2021 Jun;184(13):3573-3587.e29.

Figures

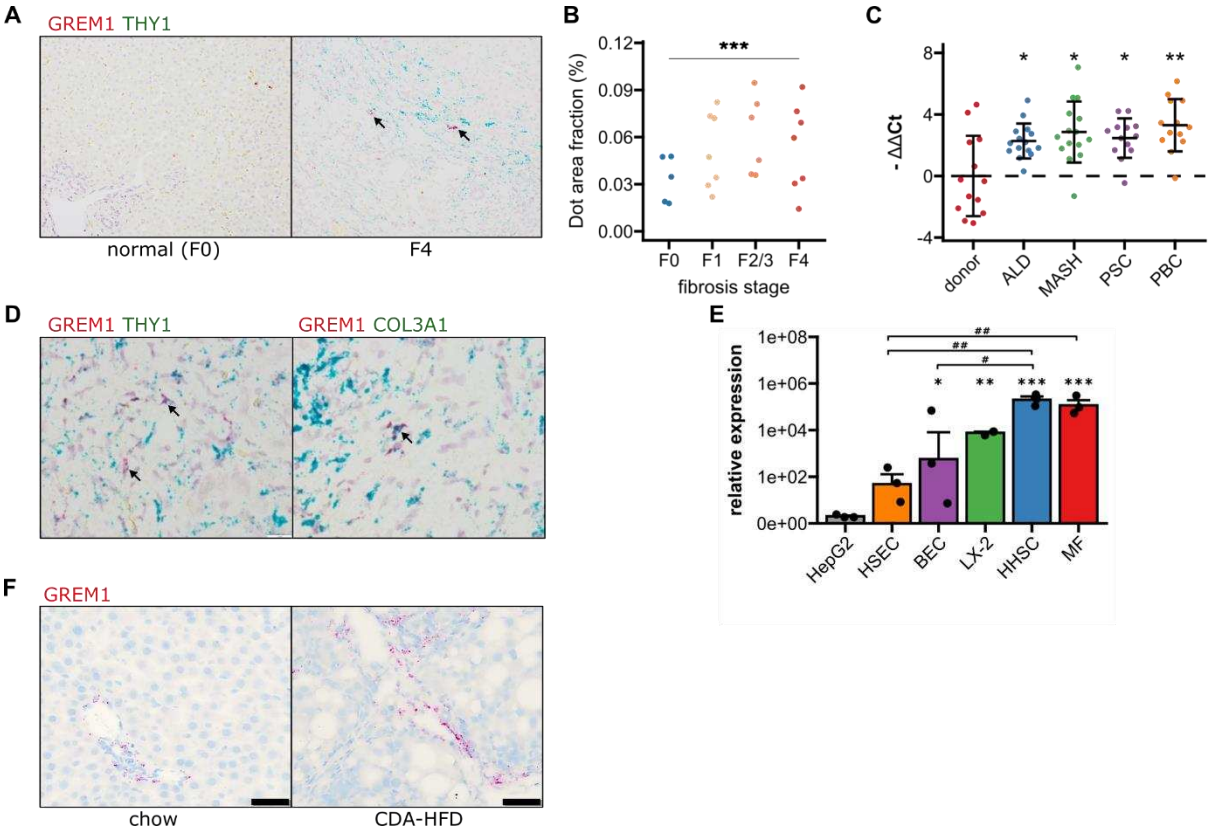

Figure 1: Validation of GREM1 expression in human and rat MASH liver fibrosis

A. Representative RNAscope in situ hybridisation (ISH) images for co-staining of GREM1 (red) and THY1 (green) in normal human liver and MASH fibrosis.
B. Quantification of ISH staining areas across different stages of liver fibrosis. Significance was assessed by two-sided Jonckheere-Terpstra test (***$p=1.3x10^{-09}$).
C. Quantification of human GREM1 qPCR across chronic liver diseases of different aetiology. Data are given as mean -ΔΔCt ± SD, relative to donor liver and normalised to the expression of SRSF4, HPRT1, and ERCC3. Significance was assessed by multiple two-sided paired Welch t-test against donor control, followed by Bonferroni-Holm adjustment (*$p<0.05$, **$p=0.004$).
D. Representative histological images of RNAscope in situ hybridisation (ISH) for co-staining of GREM1 (red) and THY1 or COL3A1 (green) in MASH fibrosis. Representative double positive cells are indicated by arrows.
E. Quantification of qPCR for GREM1 mRNA in major primary human non-parenchymal cell types. HSEC – human sinusoidal endothelial cells, BEC – biliary epithelial cells, HHSC – human hepatic stellate cells, MF – myofibroblasts.
F. Left panel shows representative RNAscope in situ hybridisation (ISH) images for GREM1 (red) in rats fed a standard chow or CDAA-HFD for 12 weeks. Right panel shows scoring of ISH staining intensity comparing livers from chow- and CDAA-HFD-fed animals.

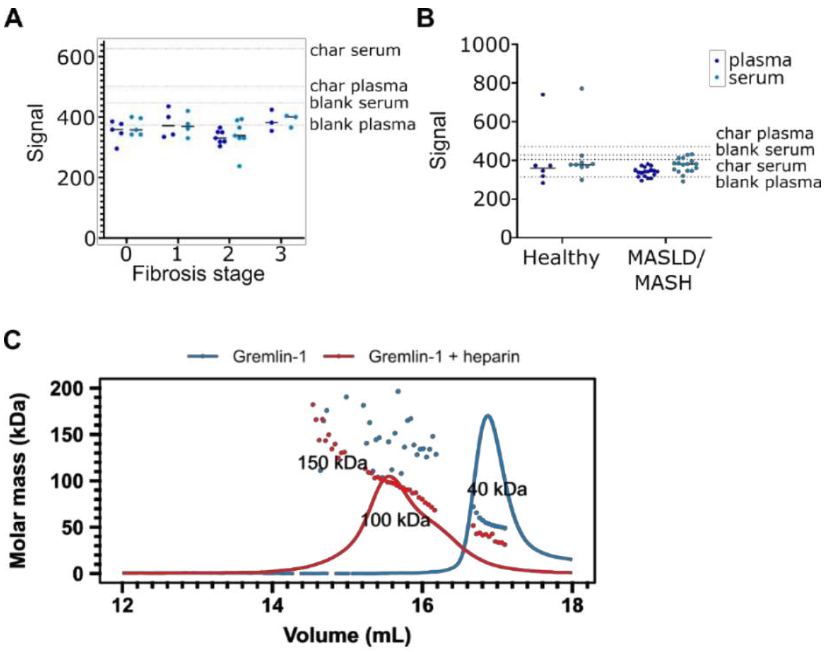

Figure 2: Circulating Gremlin-1 and evidence for heparin-binding

A. Signal for Gremlin-1 protein in the LOCI assay in serum or plasma of MASH patients at different stages of fibrosis. Char serum/plasma – charcoal stripped serum/plasma
B. Signal for Gremlin-1 protein in the LOCI assay in serum or plasma of healthy controls and MASLD/MASH. Data in A and B are given as single data points and median of luminescence signal. Dotted horizontal lines correspond to signal measured in control matrices, as given in text annotations.
C. Size exclusion chromatography for Gremlin-1 and heparin. Either gremlin-1 or gremlin-1 + heparan sulphate were run on a size exclusion chromatography column. The graph shows UV signal (continuous line) and estimated molar mass (points) on the y-axis depending on the eluting volume given on the x-axis. Text annotations give the estimated molar mass corresponding to each peak.

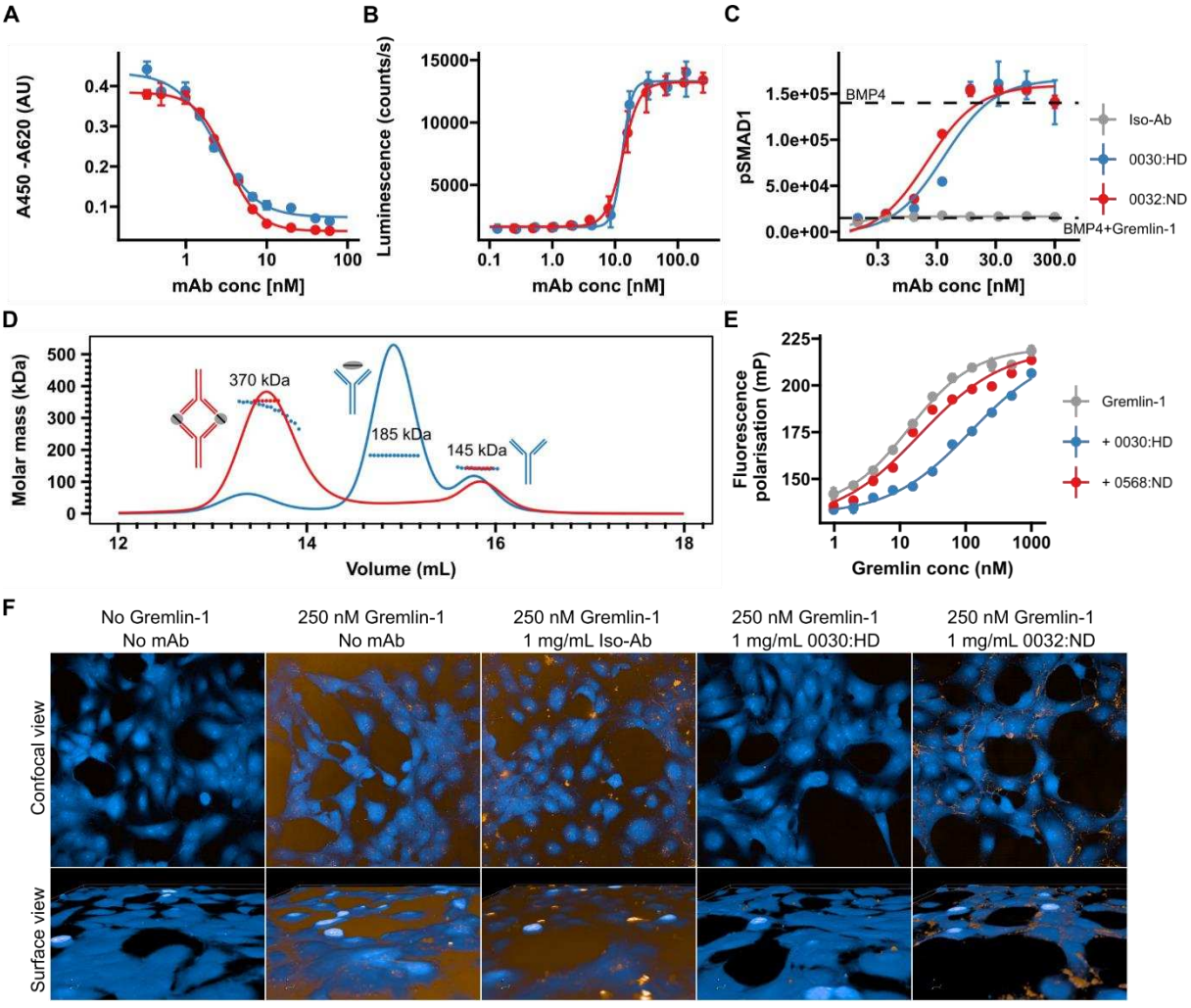

Figure 3: Validation of human recombinant anti-Gremlin-1 antibodies

A. Gremlin-1/BMP4 inhibition ELISA, measuring aG1-Ab ability to inhibit Gremlin-1 binding to BMP4. Higher absorbance indicates more Gremlin-1 binding to BMP4. IC50 = 2.7 – 3.1x10^{-9} M. Dots and error bars represent mean ± SD and lines show fitted four parameter log-logistic curve.

B. C2C12 BMP-responsive element Luc reporter gene assay. Luminescence is plotted over response to serial dilutions of anti-Gremlin-1 antibodies with higher luminescence indicating increased BMP4 activity. Dots and error bars represent mean ± SD and lines show fitted four parameter log-logistic curve. EC50 = 1.27-1.36x10^{-8}M.

C. SMAD1 phosphorylation on LX-2 cells treated with either BMP4, BMP4 and Gremlin-1 or BMP4, Gremlin-1 and serial dilutions of therapeutic antibody. Dots and error bars represent mean ± SD and lines show fitted four parameter log-logistic curve. K_D ['0032] = 2.04 nM, K_D ['0030] = 3.96 nM.

D. Size-exclusion chromatography for Gremlin-1 in combination with heparin-displacing ('0030) or non-heparin-displacing ('0032) anti-Gremlin-1 antibody. The graph shows UV signal (continuous line) and estimated molar mass (points) on the y-axis depending on the eluting volume on the x- axis. Text annotations give the estimated molar mass corresponding to each peak.

E. Fluorescence polarisation heparin-binding assay. Serial dilutions of Gremlin-1 were incubated with fixed amounts of fluorescein-heparan sulfate and 1.5-fold molar excess anti-Gremlin-1 antibody. Increased fluorescence indicates reduced mobility of heparin molecules. Dots and error bars represent mean ± SD and lines show fitted four parameter log-logistic curve. K_D [Grem1] = 13.54 nM, K_D ['0032] = 19.56 nM and K_D ['0030] = 118.65 nM.

F. Gremlin-1 cell association assay. The upper panel shows a confocal view and the lower panel a three-dimensional cell surface view for Atto-532-labelled Gremlin-1 (yellow) on LX-2 cells (labelled with CellMask Blue). Representative images for different combinations of 250 nM Gremlin-1 and isotype or anti-Gremlin-1 antibodies are given.

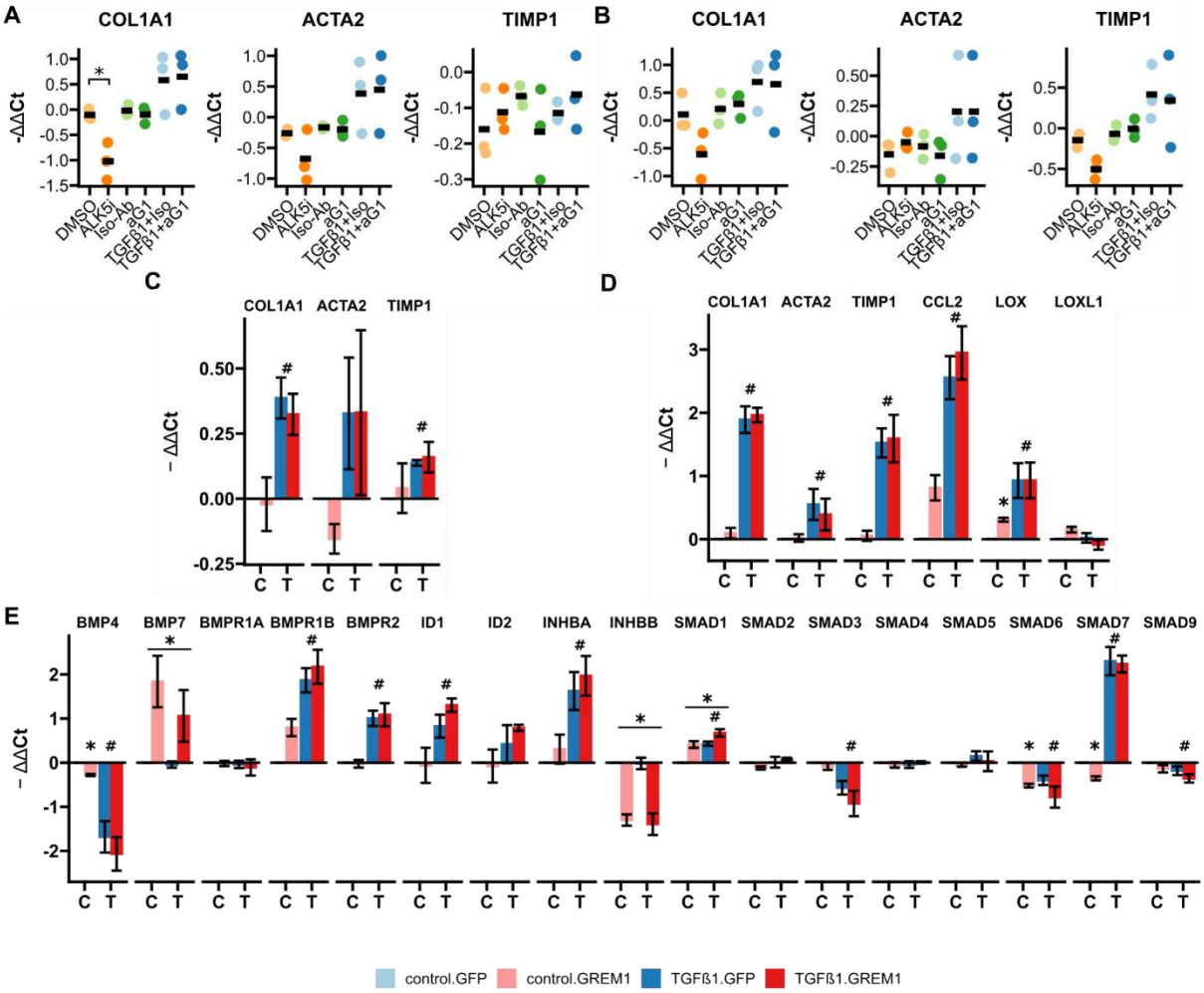

Figure 4: RTqPCR results for anti-Gremlin-1 and lenti-GREM1-treated fibrogenic cells

A. Fibrogenic marker genes in primary human hepatic stellate cells treated with anti-Gremlin-1 (aG1) or isotype control antibodies (iso-Ab).
B. Fibrogenic marker genes in primary human hepatic myofibroblasts treated with anti-Gremlin-1 or isotype control antibodies.
C. Fibrogenic gene expression in lentivirally transduced HHSC.
D. Fibrogenic gene expression in lentivirally transduced LX-2.
E. BMP signalling related gene expression in lentivirally transduced LX-2.

A-B: Data are presented as individual data points and mean for -ΔΔCt relative to untreated control and normalised to the expression of SRSF4. *p<0.05 in One-Way ANOVA and *post-hoc* paired t-tests for pre-defined comparisons with Bonferroni-Holm adjustment.

C-E: Data are given as mean ± SEM of -ΔΔCt relative to GFP and vehicle control and normalised to the expression of SRSF4. *p<0.05 in GREM1 vs GFP-control, #p<0.05 in TGFβ1 vs vehicle control in repeated measures Two-way ANOVA and post-hoc paired t-test for pre-selected comparisons and Bonferroni-Holm adjustment.

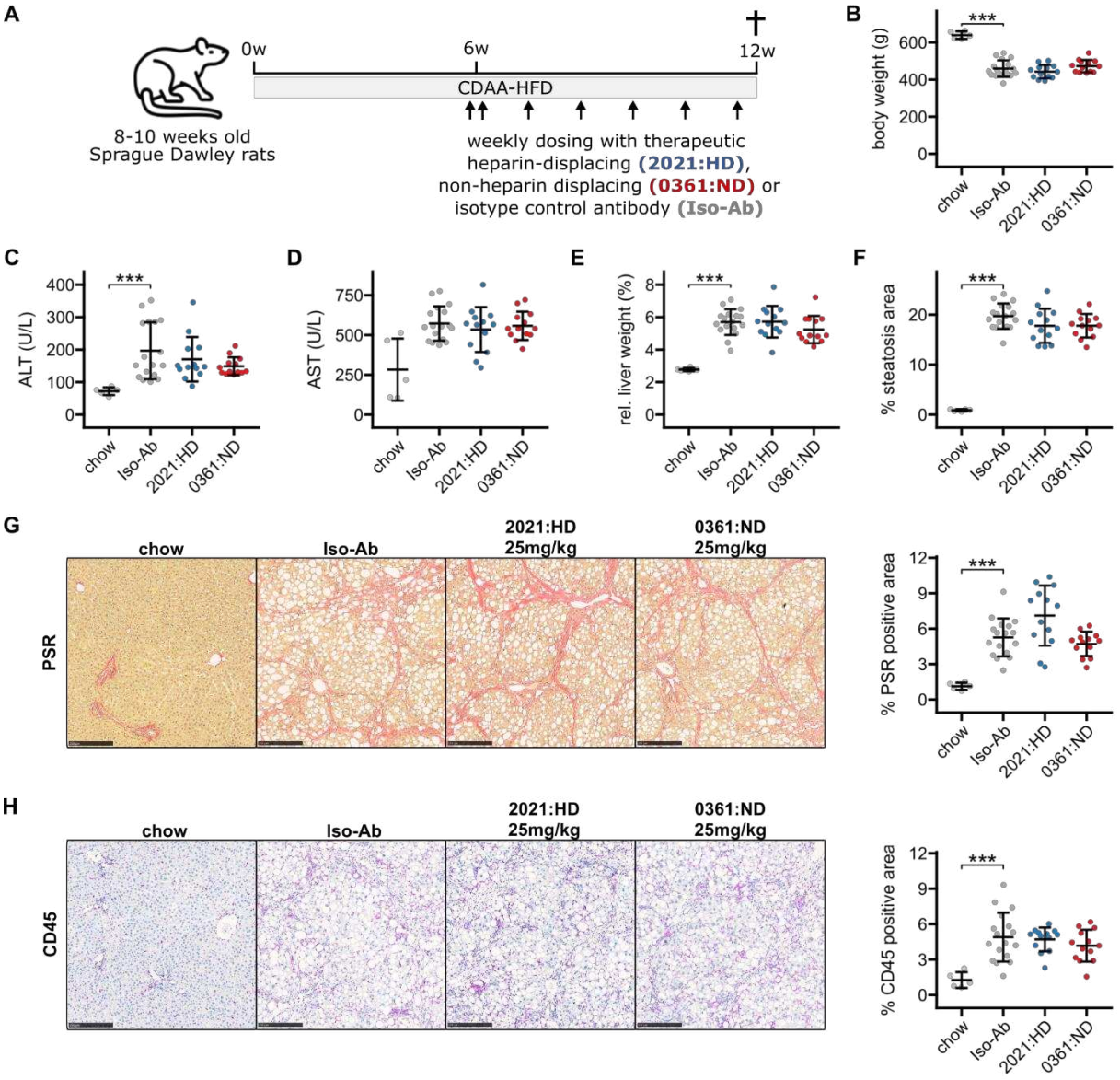

Figure 5: Results for anti-Gremlin-1 antibody treatment on CDAA-HFD induced MASH and fibrosis in rats

A. Schematic showing the study design for the animal experiment. 8-12 weeks old Sprague Dawley rats were fed a choline-deficient, L-amino acid defined high fat diet (CDAA-HFD) or standard chow for 12 weeks and treated with weekly subcutaneous injections of heparin-displacing, non-heparin-displacing or isotype control antibodies for the last 6 weeks.
B. Quantification of body weight in grams at the end of the study.
C. Quantification of plasma alanine aminotransferase (ALT) in U/L.
D. Quantification of plasma aspartate aminotransferase (AST) in U/L.
E. Quantification of relative liver weight percent of total body weight.
F. Quantification of histological liver steatosis area in percent. Data are given as mean ± SD for n=5 (chow), n=17 (Iso-Ab) and n=13 (2021 & 0361) animals per group.
G. Left panel shows representative histological images for picrosirius red staining for different treatment conditions. Scale bars represent 250 µm. Right panel shows quantification of picrosirius red staining (PSR) in percent of total area.
H. Left panel shows representative histological images for CD45 IHC for different treatment conditions. Scale bars represent 250 µm. Right panel shows quantification of CD45 IHC in percent of total area.

Data are given as mean ± SD for n=5 (chow), n=17 (Iso-Ab) and n=13 (2021 & 0361) animals per group. Significance was determined by multiple two-sided paired Welch *t*-tests against Iso-Ab, followed by Bonferroni-Holm adjustment (***p<0.001).

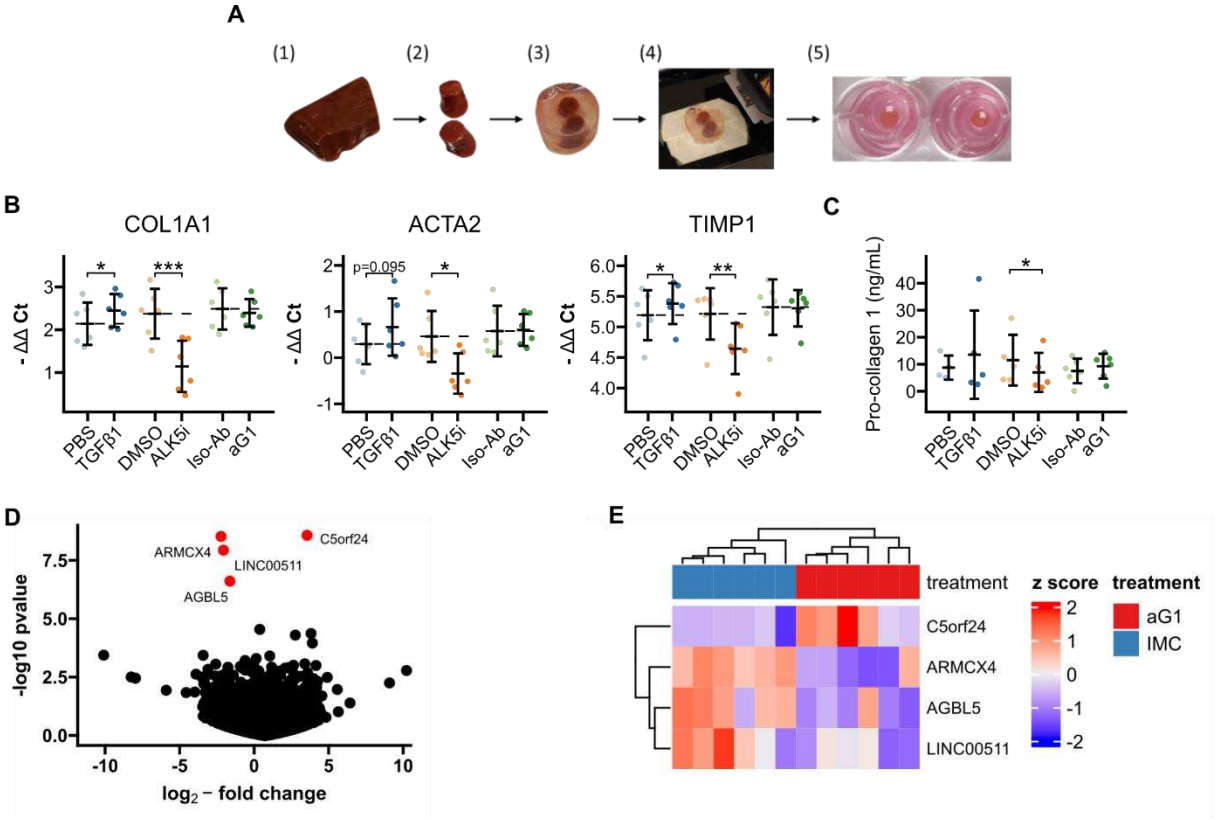

Figure 6: PCLS

A. Schematic for generation of human cirrhotic PCLS. (1) Human cirrhotic liver tissue was obtained from explants and (2) 8 mm biopsy cores were taken. (3) Tissue samples were then embedded in low-melt agarose before (4) being cut into 250 µm thin slices on a vibratome. (5) Finally, slices were incubated in 8µm 12-well inserts for 24 hours under constant agitation.
B. RTqPCR results for fibrogenic marker genes in cirrhotic PCLS. Data are given as individual data points and mean ± SD for -ΔΔ Ct relative to untreated control and normalised to the geometric mean of SRSF4, HPRT1, CTCF and ERCC expression. *p < 0.05, **p < 0.01, ***p < 0.001 in One-Way ANOVA and post-hoc paired t-tests for pre-defined comparisons with Bonferroni-Holm adjustment.
C. Pro-collagen 1 protein levels in PCLS culture supernatants. Data are given as individual data points and mean ± SD. *p < 0.05 in One-Way ANOVA and post-hoc paired t-tests for pre-defined comparisons with Bonferroni-Holm adjustment.
D. Volcano plot of differential gene expression analysis of 3' QuantSeq mRNA sequencing showing log2 -fold changes and the negative decadic logarithm of unadjusted p-values for all expressed genes in aG1 vs Iso-Ab treated PCLS. Significantly regulated genes (i.e. adj. p-value < 0.05) are labelled and marked in red.
E. Heatmap showing centred and scaled gene expression for significantly regulated genes.

The anti-Gremlin-1 antibody (aG1) used for experiments in panels B and C was the 0030:HD antibody.

1226 # Tables and their legends

1227

1228 **Table 1: Clinical baseline characteristics of the FLINC cohort (Fig. 2A and B)**

	Control (N =6)	MASLD (n = 19)	p
Age, years	45.5 (27.3-63.0)	56.0 (45.5-60.0)	0.36*
Sex (Female), N(%)	3 (50)	0 (47.4)	1**
Diabetes, N(%)		10 (52.6)	
Hypertension, N(%)		10 (52.6)	
Dyslipidaemia, N(%)		10 (52.6)	
BMI	23.1 (22.5-24.7)	30.6 (28.3-33.4)	0.0001*
NAS		5 (4-6)	
Fibrosis stage, N(%) 0 1 2 3		 5 (26.3) 4 (21.1) 7 (36.8) 3 (15.8)	

1229 Continuous data: median with p25-p75

1230 *Mann-Whitney U test

1231 ** fisher's test

1232

Supplementary Material

Evaluation of Gremlin-1 as a therapeutic target in metabolic dysfunction-associated steatohepatitis

Paul Horn, Jenny Norlin, Kasper Almholt, Birgitte M. Viuff, Elisabeth D. Galsgaard, Andreas Hald, Franziska Zosel, Helle Demuth, Svend Poulsen, Peder L. Norby, Morten G. Rasch, Mogens Vyberg, Marco R. Rink, Emma Shepherd, Ellie Northall, Patricia F. Lalor, Chris J. Weston, Morten Fog-Tonnesen and Philip N. Newsome

Supplementary Tables

Supplementary Table 1: Rat CDAA-HFD study: clinical chemistry and histological results for all antibody concentrations

	chow	Iso-Ab	2021				0361		
			25	2.5	1	0.25	25	2.5	1
body weight (g)	639±20	459±45	443±36	438±36	442±28	447±42	473±33	453±41	446±47
ALT (U/mL)	72±12	197±88	170±69	247±209	155±47	194±66	149±28	170±34	191±71
AST (U/mL)	283±195	572±108	534±141	551±101	522±82	607±103	558±89	518±157	587±114
relative liver weight (%)	2.77±0.11	5.7±0.79	5.72±0.97	5.79±1.12	6.03±0.86	5.45±0.82	5.24±0.84	5.58±1.01	5.48±0.82
steatosis (% area)	0.85±0.23	19.7±2.53	17.77±3.41	18.46±3.36	18.36±3.46	16.76±3.01	17.78±2.35	19.25±2.66	18.12±3.54
PSR (% area)	1.12±0.31	5.26±1.61	7.11±2.54	5.58±2.82	6±2.83	5.78±2.62	4.71±1.03	5.54±2.36	6±2.59
CD45 (% area)	1.26±0.67	4.89±2.07	4.7±1.01	4.03±1.14	5.87±2.68	7.18±2.8	4.17±1.35	5.81±3.76	4.74±2.07
Collagen 1 (% area)	2.59±1.47	10.9±2.6	13.62±3.14	13.15±6.51	13.37±4.44	14.35±6.42	10.49±2.68	11.32±4.14	12.62±4.46
aSMA (% area)	0.83±0.16	13.15±3.16	13.75±2.41	11.82±2.42	14±2.67	13.56±3.14	12.25±2.68	12.84±2.05	13.43±2.88
CD68 (% area)	3.79±0.5	14.45±2.37	15.16±2.11	14.81±3.35	14.69±2.72	15.73±3.27	13.34±2.4	14.14±2.91	14.49±2.51
CD11b (% area)	0.07±0.04	0.68±0.53	0.84±0.71	0.54±0.42	0.91±0.57	0.96±0.89	0.67±0.5	0.9±0.89	0.75±0.59

All data are given as mean ± SD

Supplementary Table 2: Rat CDAA-HFD study: qPCR results for all antibody concentrations

	chow	Iso-Ab	2021				0361		
			25	2.5	1	0.25	25	2.5	1
Col1a1	0±1.13	6.97±0.78	6.95±0.71	6.82±0.63	7.12±0.95	7.39±0.57	7.09±0.69	7.03±0.73	6.97±0.78
Col3a1	0±0.72	3.63±0.68	3.4±0.48	3.58±0.54	3.81±0.58	3.97±0.39	3.77±0.37	3.75±0.52	3.79±0.8
Grem1	0±0.51	3.33±0.55	3.37±0.37	3.28±0.36	3.66±0.64	3.75±0.46	3.49±0.39	3.47±0.35	3.42±0.35
Mki67	0±0.52	4.53±0.54	4.59±0.46	4.54±0.69	4.83±0.71	4.59±0.57	4.79±0.54	4.55±0.6	4.27±0.61
Tgfb1	0±1.14	4.12±1.32	4.44±0.62	4.24±0.83	4.02±2.17	4.57±0.53	4.08±1.11	4.35±0.65	4.5±0.64
Timp1	0±0.25	4.35±0.36	4.5±0.36	4.36±0.51	4.5±0.61	4.47±0.29	4.3±0.4	4.26±0.35	4.35±0.4
Tnf	0±1.22	2.96±1.13	3.52±1.09	3.1±0.78	3.55±0.99	3.82±1.11	3.54±0.77	3.46±0.95	3.61±0.91

All data are given as mean ± SD

Supplementary Table 3: Table of Taqman Assay IDs

Species	Target	Assay ID
Human	ACTA2	Hs01879841_s1
	AFTPH	Hs00214281_m1
	BMP2	Hs00154192_m1
	BMP4	Hs00370078_m1
	BMP7	Hs00233476_m1
	BMPR1A	Hs04980288_g1
	BMPR1B	Hs01010965_m1
	BMPR2	Hs00176148_m1
	COL1A1	Hs00164004_m1
	CTCF	Hs00902016_m1
	ERCC3	Hs01554457_m1
	GREM1	Hs01879841_s1
	HPRT1	Hs02800695_m1
	ID1	Hs00357821_g1
	ID2	Hs00747379_m1
	INHBA	Hs01081598_m1
	INHBB	Hs00173582_m1
	SMAD1	Hs00195432_m1
	SMAD2	Hs00998187_m1
	SMAD3	Hs00969210_m1
	SMAD4	Hs00929647_m1
	SMAD5	Hs00195437_m1
	SMAD6	Hs00178579_m1
	SMAD7	Hs00998193_m1
	SMAD9	Hs00931723_m1
	SRSF4	Hs00194538_m1
	TIMP1	Hs01092512_g1
Rat	B2m	Rn00560865_m1
	Actb	Rn00667869_m1
	Gapdh	Rn01775763_g1
	Col3a1	Rn01437681_m1
	Col1a1	Rn01463848_m1
	Tgfb1	Rn00572010_m1
	Mki67	Rn01451446_m1
	Timp1	Rn01430873_g1
	TNF	Rn99999017_m1
	Grem1	Rn01509832_m1

All Taqman assays were purchased from ThermoFisher Scientific

1257 **Supplementary Table 4: Custom-made primer sequences**

Target	Primer	Sequence
GAPDH	GAPDH_116bp_fw	5' - CTC TGC TCC TCC TGT TCG AC - 3'
	GAPDH_116bp_rv	5' - CAA TAC GAC CAA ATC CGT TGA C - 3'
GFP	GFP_109bp_fw	5' - GCT ACC CCG ACC ACA TGA AG - 3'
	GFP_109bp_rv	5' - CGG GTC TTG TAG TTG CCG T - 3'
GREM1	GREM1_109bp_fw	5' - GAG CCC TGC TTC TCC TCT TG - 3'
	GREM1_109bp_rv	5' - TCT GAG TCA TTG TGC TGG GC - 3'

Supplementary Figures

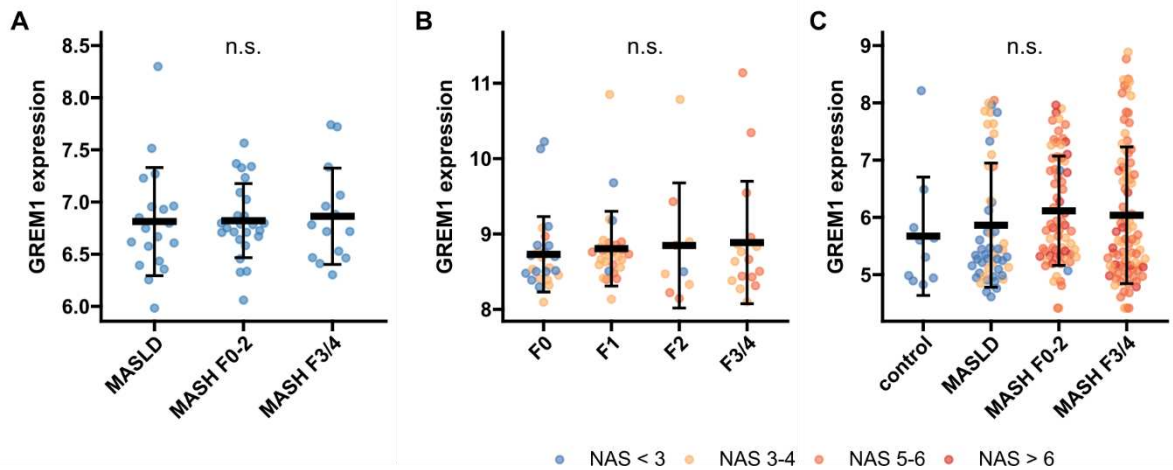

Supplementary Figure 1: GREM1 gene expression in public bulk RNAseq data from human MASLD liver

A. E-MTAB-9815 (n = 58).
B. GSE130970 (n = 78).
C. GSE135251 (n = 216).

All data are given as individual data points and mean±SD of variance stabilised expression as obtained from the vst function in DESeq2.

n.s. – not significant, statistical significance was tested using the likelihood ratio test and Benjamini Hochberg correction in DESeq2.

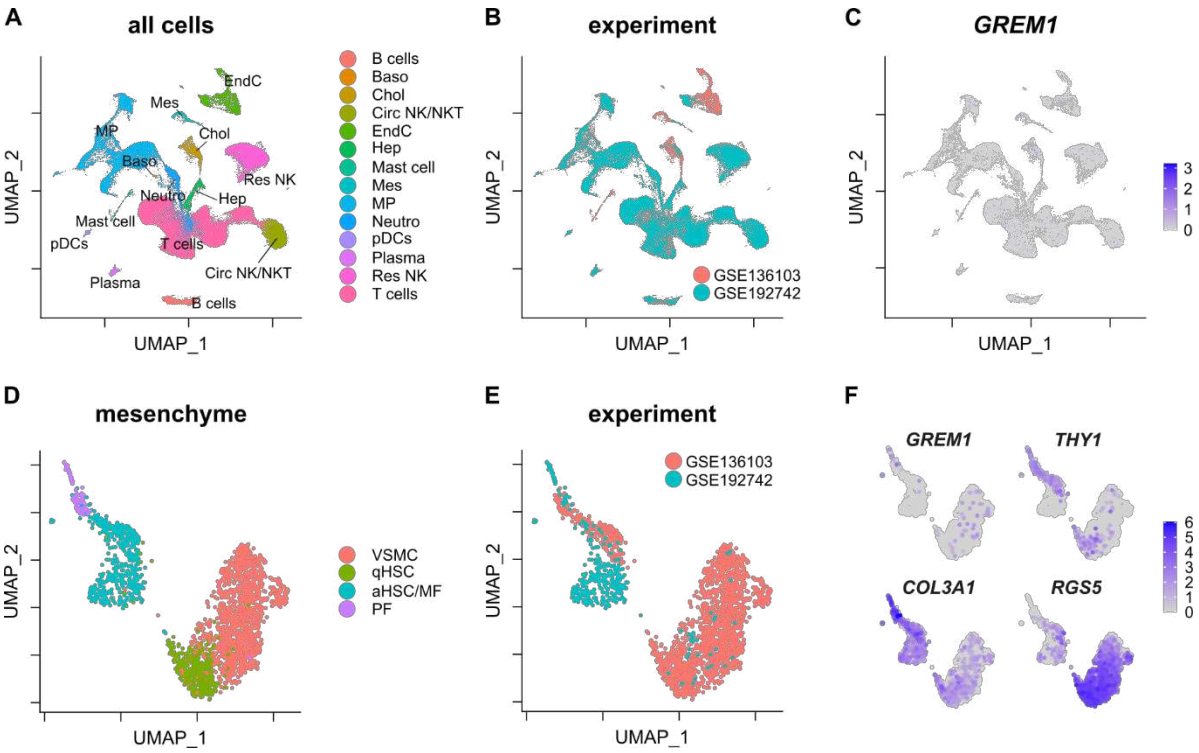

Supplementary Figure 2: GREM1 expression in publicly available human scRNA-seq data

A. UMAP representation of all cells in GSE136103 and GSE192742 scRNA-sequencing datasets. Cells are coloured by cell type identity.
B. UMAP representation of all cells in GSE136103 and GSE192742 scRNA-sequencing datasets. Cells are coloured by experiment.
C. Log_2-normalised GREM1 gene expression in all cells.
D. UMAP representation of mesenchymal cells in GSE136103 and GSE192742 scRNA-sequencing datasets. Cells are coloured by cell cluster identity.
E. UMAP representation of mesenchymal cells in GSE136103 and GSE192742 scRNA-sequencing datasets. Cells are coloured by experiment.
F. Log_2-normalised gene expression of GREM1, THY1, COL3A1 and RGS5 in mesenchymal cells.

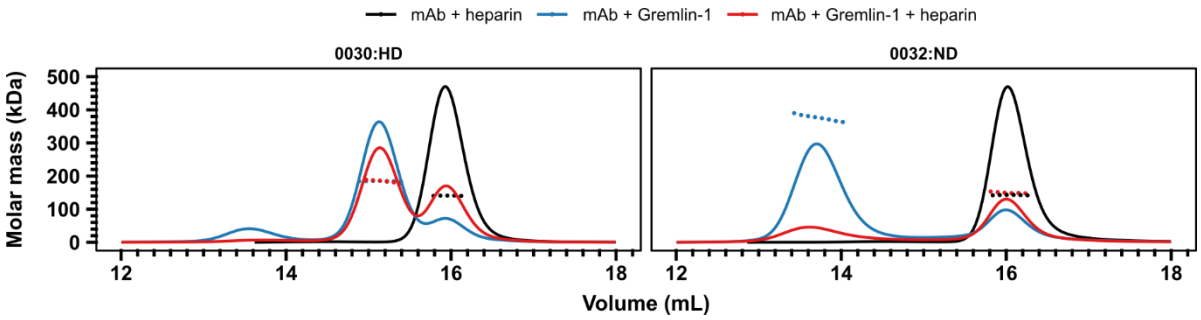

Supplementary Figure 3: Size-exclusion chromatography for Gremlin-1-anti-Gremlin-1-heparin complexes

Different combinations of heparin-displacing ('0030, left) or non-displacing ('0032, right) therapeutic anti-Gremlin-1 antibodies with heparin alone, Gremlin-1 alone or Gremlin-1 and heparin were run on a size exclusion chromatography column. The graph shows UV signal (continuous line) and estimated molar mass (points) on the y-axis, depending on the eluting volume on the x-axis. The low recovery of 0032/Gremlin-1/heparin complexes was accompanied by visual precipitation in the sample vial, indicating the formation of macroscopic insoluble complexes.

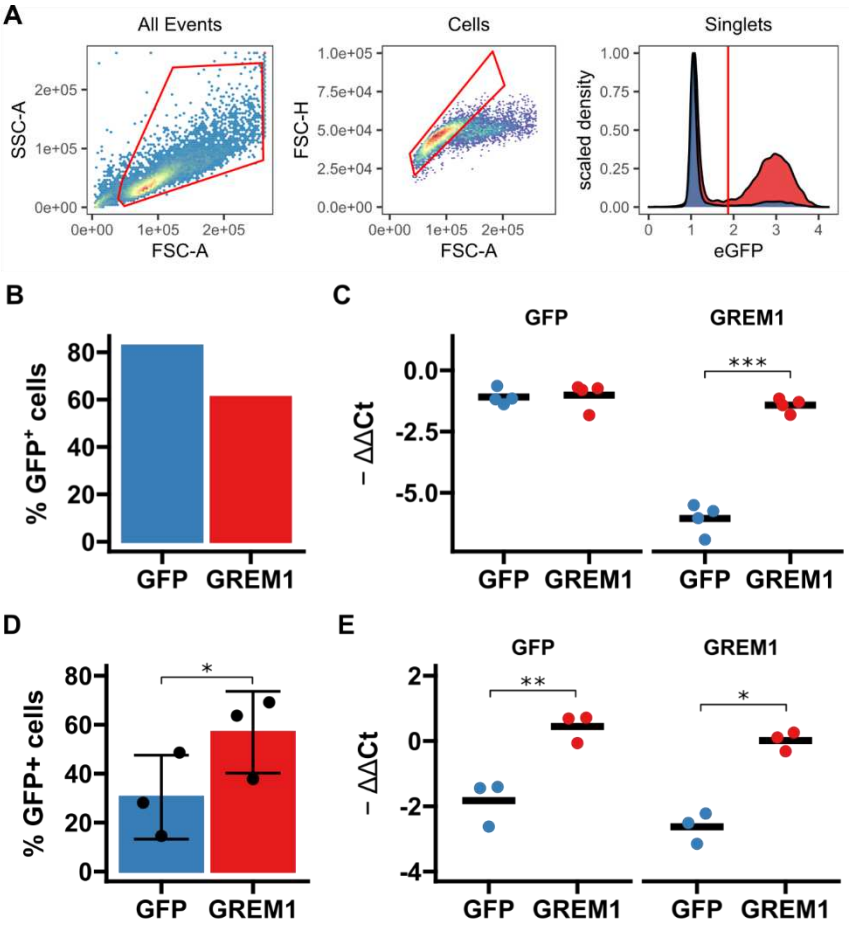

Supplementary Figure 4: Validation of GREM1 overexpression in LX-2 and HHSC by flow cytometry and RTqPCR.

A. Gating strategy for flow sorting of lentivirally transduced cells. First, cells were selected (left panel) before gating on singlets (middle panel). Cells were then gated based on the 99 percent percentile of non-transduced cells to identify cells positive for GFP (right panel). Red polygons show gates and the red vertical line in the right panel shows the cut-off for GFP positivity.
B. Bar diagram showing percentage of GFP-positive cells in GREM1 or GFP-control lentivirally transduced LX-2, n = 1.
C. SybrGreen RTqPCR results for GFP and GREM1 mRNA in lentivirally transduced LX-2, n = 4.
D. Bar diagram showing percentage of GFP-positive cells in GREM1 or GFP-control lentivirally transduced HHSC, n = 3.
E. SybrGreen RTqPCR results for GFP and GREM1 mRNA in lentivirally transduced HHSC, n = 3.
F. Data in B and D are given as individual data points and mean±SD; data in C and E are given as individual data points and mean. *p < 0.05, **p < 0.01 and ***p < 0.001 in paired two-sided t-test.

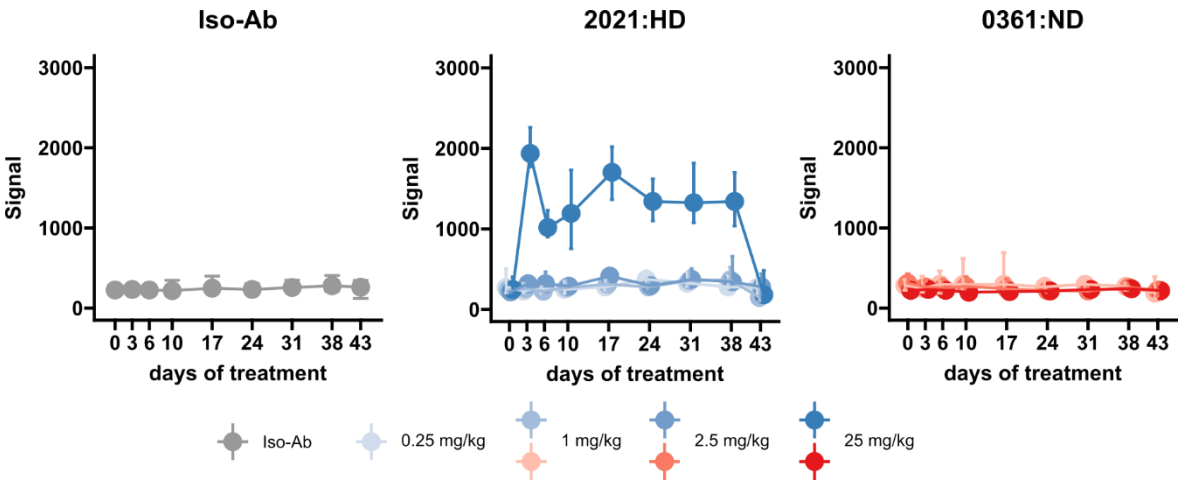

Supplementary Figure 5: Target engagement studies in the rat CDA-HFD model

Peripheral blood samples were taken before first antibody injection and at different timepoints during treatment, as indicated on the x-axes. Plots show signal intensity for Gremlin-1 protein in plasma by alphaLISA. All data are given as median and IQR.

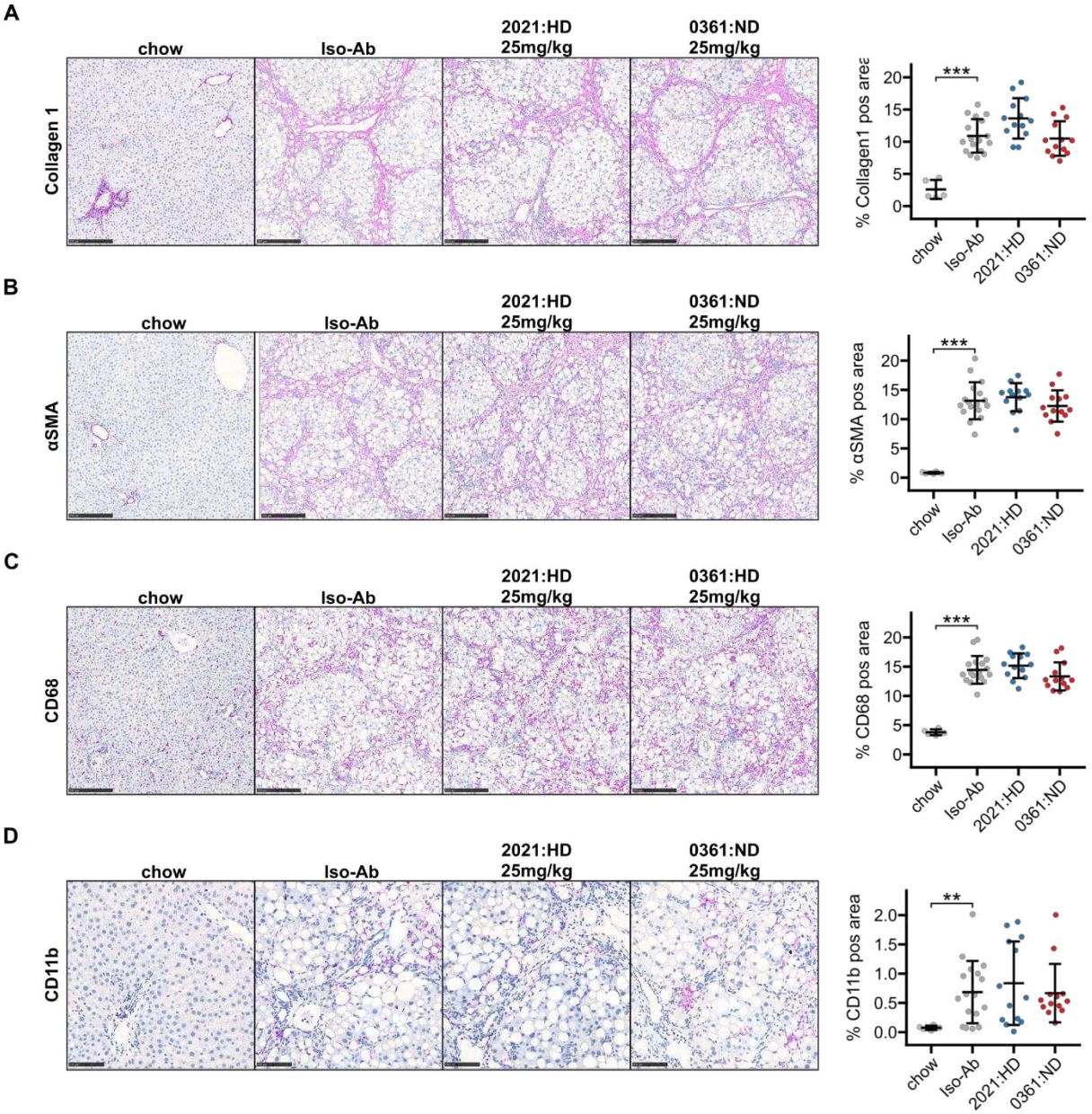

Supplementary Figure 6: Additional IHC data from rat CDAA-HFD study

A. Left panel shows representative histological images for Collagen 1 IHC for different treatment conditions. Scale bars represent 250 µm. Right panel shows quantification of Collagen 1 staining in percent of total area.
B. Left panel shows representative histological images for alpha smooth muscle actin (αSMA) IHC for different treatment conditions. Scale bars represent 250 µm. Right panel shows quantification of αSMA staining in percent of total area.
C. Left panel shows representative histological images for CD68 IHC for different treatment conditions. Scale bars represent 250 µm. Right panel shows quantification of CD68 staining in percent of total area.
D. Left panel shows representative histological images for CD11b IHC for different treatment conditions. Scale bars represent 100 µm. Right panel shows quantification of CD11b staining in percent of total area.

Data are given as mean ± SD for n=5 (chow), n=17 (Iso-Ab) and n=13 (2021 & 0361) animals per group. Significance was determined by multiple two-sided paired Welch t-tests against Iso-Ab, followed by Bonferroni-Holm adjustment (**p<0.01, ***p<0.001).

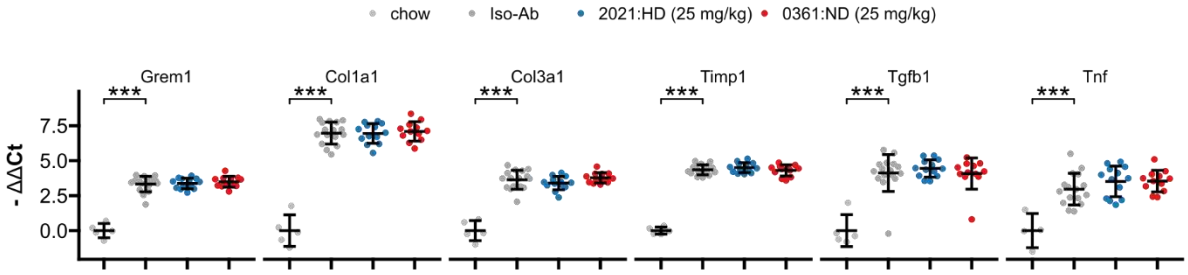

Supplementary Figure 7: RTqPCR results for anti-Gremlin-1 antibody treatment on CDAA-HFD induced MASH and fibrosis in rats

Data are given as single data points and mean ± SEM for -ΔΔCt relative to chow control and normalised to B2m expression. ***p<0.001 in One-Way ANOVA and post-hoc Dunnett test compared to Iso-Ab treated animals.

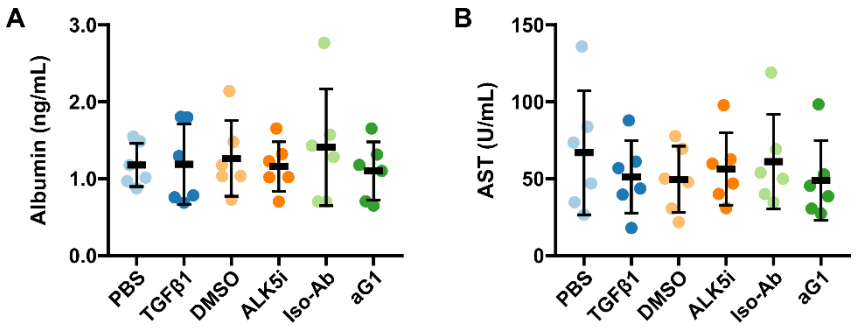

Supplementary Figure 8: AST and Albumin levels in precision-cut liver slices supernatants

A. Albumin levels in supernatants of treated PCLS.
B. AST enzymatic activity in supernatants of treated PCLS.

The anti-Gremlin-1 antibody (aG1) used for experiments was the 0030:HD antibody. Data are given as individual data points (coloured points) and mean ± SD for n = 6 per treatment condition.

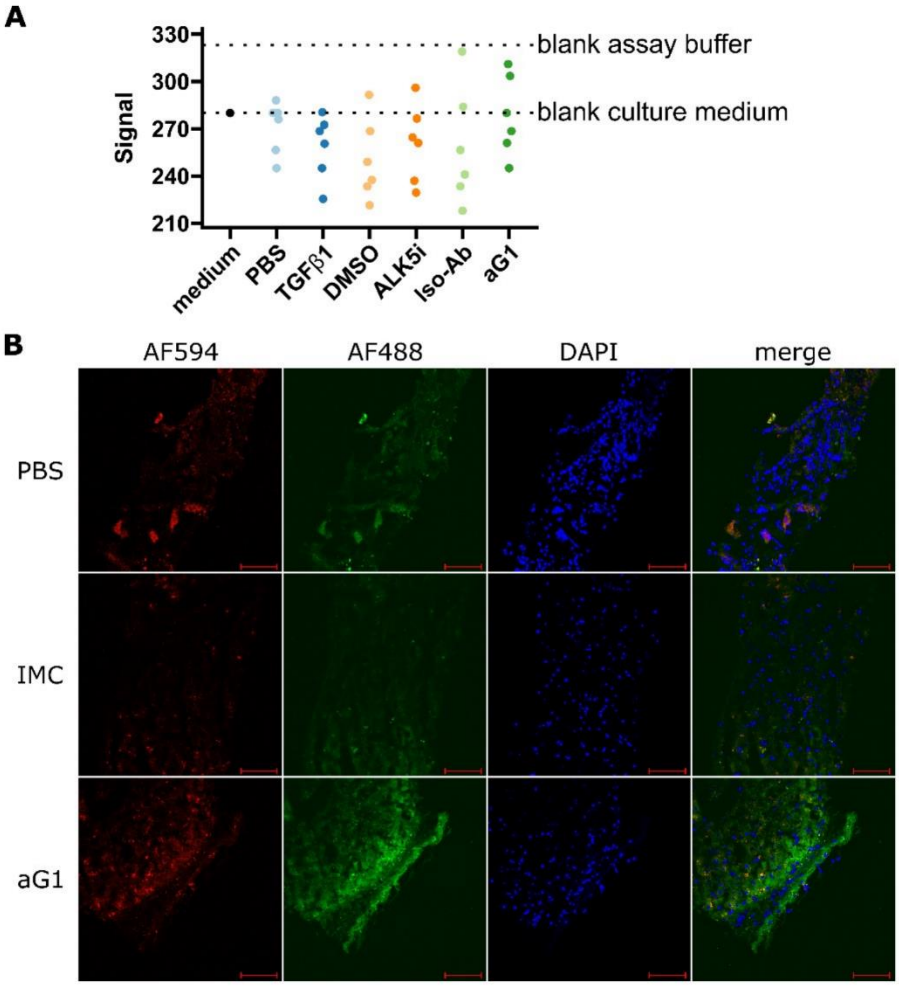

Supplementary Figure 9: Target engagement studies in PCLS.

A. Results of alphaLISA for Gremlin-1 protein in supernatants of treated cirrhotic PCLS. Data are given as individual data points for fluorescent signal intensity and dotted lines indicate the signal intensities obtained using blank culture medium or blank assay buffer.

B. One set of cirrhotic PCLS was treated with either PBS or AF488-conjugated non-heparin displacing isotype control or anti-Gremlin-1 antibody for 24 h. Unfixed frozen sections were imaged after autofluorescence quenching and staining with DAPI. Red autofluorescence was detected using the AF594 channel. Scale bar represents 100 µm.

The anti-Gremlin-1 antibody (aG1) used for experiments in panels A was the 0030:HD antibody, the aG1 used for B was the 0032:ND antibody.